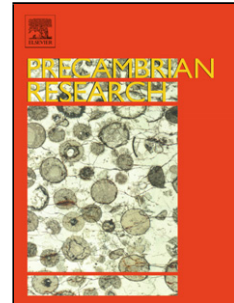


Accepted Manuscript

Title: The origin of microcontinents in the Central Asian Orogenic Belt: Constraints from paleomagnetism and geochronology.

Authors: Natalia M. Levashova, Joseph G. Meert, Anatoly S. Gibsher, Warren C. Grice, Mikhail L. Bazhenov



PII: S0301-9268(10)00303-7
DOI: doi:10.1016/j.precamres.2010.12.001
Reference: PRECAM 3320

To appear in: *Precambrian Research*

Received date: 7-6-2009
Revised date: 2-12-2010
Accepted date: 3-12-2010

Please cite this article as: Levashova, N.M., Meert, J.G., Gibsher, A.S., Grice, W.C., Bazhenov, M.L., The origin of microcontinents in the Central Asian Orogenic Belt: Constraints from paleomagnetism and geochronology., *Precambrian Research* (2010), doi:10.1016/j.precamres.2010.12.001

This is a PDF file of an unedited manuscript that has been accepted for publication. As a service to our customers we are providing this early version of the manuscript. The manuscript will undergo copyediting, typesetting, and review of the resulting proof before it is published in its final form. Please note that during the production process errors may be discovered which could affect the content, and all legal disclaimers that apply to the journal pertain.

The Central Asian Orogenic Belt (CAOB) is widely recognized as a locus of Asia's main growth during the Neoproterozoic – Paleozoic, but its evolution remains controversial. The views on the most enigmatic, late Neoproterozoic to Cambrian, stages are critically dependent on the origin and subsequent kinematics of numerous microcontinents that comprise the structure of Kazakhstan, Tien Shan, Altai and Mongolia.

We report new paleomagnetic data and U-Pb zircon ages from Neoproterozoic volcano-sedimentary rocks from the Lesser Karatau block in central Kazakhstan. The laser ablation U-Pb age of felsic tuff of the Kurgan Fm. is 766 ± 7 Ma. Thermal demagnetization revealed that most studied samples retained a dual-polarity pre-tilting component whose primary origin is supported by a conglomerate test. According these paleomagnetic data, the Lesser Karatau microcontinent was located at a paleolatitude of $34.2^\circ \pm 5.3^\circ$, N or S, at about 770 Ma. There is only one additional CAOB microcontinent, the Baydaric microcontinent in central Mongolia, for which reliable paleomagnetic data indicate a paleolatitude of $47^\circ \pm 14^\circ$, N or S, at about 770-805 Ma (Levashova et al., 2010).

Several lines of evidence favor the view that the above CAOB microcontinents were originally parts of two larger domains, thus allowing extrapolation of the above paleomagnetic data to much larger territories, the Kazakhstan and Mongol domains that, in turn, might have belonged to major cratonic areas. A comparison of our paleomagnetic data with those from the larger cratonic nuclei provides first-order constraints on the origins of the CAOB microcontinents. . We compare the existing tectonostratigraphic correlations between the Neoproterozoic to early Paleozoic sections of the microcontinents with coeval sections on the margins of Tarim, Australia, South China, Siberia, and North China. This combined analysis excludes a southern hemispheric location for the CAOB microcontinents at 750-800 Ma. Of the several cratons that were located in the northern hemisphere at that time we favor a hypothesis that the Kazakhstan and Mongol domains had originally belonged either to Tarim or South China.

The origin of microcontinents in the Central Asian Orogenic Belt: Constraints from paleomagnetism and geochronology.

Natalia M. Levashova^a, Joseph G. Meert^b, Anatoly S. Gibsher^c,
Warren C. Grice^b, and Mikhail L. Bazhenov^a

^a*Geological Institute, Academy of Science of Russia, Pyzhevsky Lane, 7, Moscow 109017, Russia*

^b*Department of Geological Sciences, 274 Williamson Hall, Gainesville, FL 32611 USA*

^c*Institute of Geology and Mineralogy, Siberian Branch of the Academy of Science of Russia,
Koptug Pr. 3, Novosibirsk 630090, Russia*

1. Introduction

The Central Asian Orogenic Belt (CAOB) stretches from the Urals via Kazakhstan, the Tien Shan, Altai, and Mongolia to the Pacific. The central part of the belt is located between the East European, Siberian, and Tarim cratons (Fig. 1a) and has a complex tectonic history. Unlike many intra- or peri-continental orogenic belts such as the Urals, Andes, and Appalachians, no prevailing structural trend is observed here. Numerous microcontinents with Precambrian basement and late Neoproterozoic - early Paleozoic clastic - carbonate cover are tectonically juxtaposed with late Neoproterozoic - early Paleozoic subduction-related volcanic complexes, accretionary wedges, and flysch sequences (Mossakovsky et al., 1993). The middle – late Paleozoic structural pattern of the CAOB is dominated by long, strongly curved subduction-related volcanic belts that unconformably overlie the older structures.

Most authors acknowledge the important role of the CAOB in the formation of Eurasia, and a number of contrasting models were proposed to explain its evolution. Notable syntheses (e.g. Zonenshain et al. 1990; Mossakovsky et al. 1993; Didenko et al. 1994; Kheraskova et al. 2003; Khain et al. 2003; Windley et al., 2007) regard the CAOB as an ancient analogue to the setting in the modern western Pacific. These authors argue that the CAOB was formed by the closure of the Paleo-Asian Ocean, where an archipelago of scattered Precambrian microcontinents, oceanic basins and island arcs existed in the late Neoproterozoic– early Paleozoic.

Some models advocate the existence of a long-living volcanic arc system in the paleo-Asian ocean (Sengör and Natal'in, 1996; Puchkov, 2000; Yakubchuk, 2008; Yakubchuk et al., 2002; Stampfli and Borel, 2002). For instance, Sengör and Natal'in (1996) assumed that there was a long, continuous 'Kipchak Arc' connecting Siberia and Baltica in the late Neoproterozoic -

34 early Paleozoic. From the latest Ordovician to the Permian, fragments of the ancient arc were
35 imbricated and gradually amalgamated into a continent-sized domain (Kazakhstan continent).

36 None of the existing models explains all available data on CAOB geology (e.g., Windley
37 et al. 2007). Biostratigraphic evidence does not adequately discriminate between the models as
38 the spatial distribution of some taxa better match one type of model, whereas other taxa favor a
39 different model (Burtman, 1999). It is possible that the use of paleomagnetic data may offer
40 some resolution between the myriad models proposed for the evolution of the CAOB; however,
41 the present database is too populated for distinguishing between the many models.

42 If we are to reconstruct the tectonic evolution of the CAOB, then we must begin by
43 establishing the Neoproterozoic – Cambrian history of its development because different choices
44 for the starting point will lead to dissimilar Paleozoic reconstructions. However, these early
45 phases remain both enigmatic and contentious. For instance, the overall stratigraphic similarities
46 between late Neoproterozoic – Cambrian sections on many CAOB microcontinents were noticed
47 decades ago (Ankinovich, 1961; Zubtsov, 1971), but disparate interpretations were inferred.
48 Some authors assumed that the microcontinents rifted from East Gondwana in the
49 Neoproterozoic and moved as a loose agglomeration across the Paleo-Asian Ocean until
50 collision with either Siberia or each other (Mossakovsky et al. 1993; Didenko et al. 1994;
51 Kheraskova et al., 2003). In contrast, Berzin and Dobretsov (1994) suggested that all these
52 blocks rifted from Siberia in the late Neoproterozoic and re-docked with Siberia in Ediacaran
53 time. Sengör and Natal'in (1996) proposed, albeit implicitly, that all microcontinents rifted from
54 either Siberia or Baltica in the Ediacaran.

55 Paleomagnetic data from the CAOB microcontinents are invaluable for documenting
56 their origin and subsequent kinematics; however, such data are scarce. Evans et al. (1996)
57 studied carbonates of the early Cambrian Bayan-Gol Formation on the Baydaric (Dzabkhan in
58 other publications) microcontinent in central Mongolia but could only isolate an overprint. The
59 same formation and carbonates of the Ediacaran - Nemakit-Daldynian Tsagan-Oloom Formation
60 were studied by Kravchinsky et al. (2001) who, in addition to the overprint, isolated a dual-
61 polarity component from both formations. These data are highly scattered and are not supported
62 by any field tests, nevertheless, the authors advocate a primary origin for the result. According to
63 Kravchinsky et al. (2001), the Baydaric microcontinent was located near the equator in
64 Ediacaran-early Cambrian times. Kravchinsky et al. (2010) also present paleomagnetic data from
65 Tuva-Mongolia with similar results; namely, a predominant Paleozoic overprint and an inferred
66 ancient magnetization of Ediacaran-Cambrian age. The Ediacaran-Cambrian directions have a
67 shallow inclination suggesting near-equatorial paleolatitudes for Tuva-Mongolia and the
68 Baydaric microcontinents. Minimal paleomagnetic data from Lesser Karatau (Tamdy Series)

69 also indicates a possible low latitude Cambrian-Ordovician position (Pradhan et al., 2009). So far
70 the only other Neoproterozoic paleomagnetic result on the CAO B microcontinents is published
71 by Levashova et al.(2010) who studied Neoproterozoic volcanic rocks from the Baydaric
72 microcontinent (star in Fig. 1b). New paleomagnetic and geochronological data enabled these
73 authors to conclude that about 770-805 Ma ago the Baydaric domain was located at a latitude of
74 $47 \pm 14^\circ$ N or S.

75 We present new paleomagnetic data and U-Pb zircon ages for Neoproterozoic volcano-
76 sedimentary rocks of another CAO B microcontinent, the Lesser Karatau block in central
77 Kazakhstan (Fig. 1b), and discuss tectonic implications of these new results.

78

79 **2. The Precambrian basement in the CAO B**

80 Precambrian microcontinents within the CAO B cluster mostly in the western part of
81 Central Kazakhstan and to the south of the Siberian craton (Fig. 1b). These microcontinents
82 include the the Kokchetav, Ulutau, Karatau-Talas, North Tien Shan, Aktau-Mointy sialic massifs
83 and several smaller blocks. The overall stratigraphic similarities between late Neoproterozoic –
84 Cambrian sections of these microcontinents were noticed decades ago (e.g. Ankinovich, 1961;
85 Zubtsov, 1971). The basement of these massifs typically consists of Paleoproterozoic
86 metamorphic complexes that are overlain by thick piles of Neoproterozoic quartzite and schist
87 with minor carbonates (Degtyarev and Ryazantsev, 2007). The Archean to Paleoproterozoic age
88 of the crystalline basement is demonstrated for several blocks, including the Kokchetav and
89 Ulutau microcontinents, as compiled by Kröner et al. (2007). Detrital zircons with similarly old
90 ages were found in sedimentary sequences from these microcontinents (Kröner et al., 2007). In
91 some microcontinents the available oldest reported ages are much younger: 880 ± 11 Ma in the
92 Aktau-Mointy microcontinent (multigrain zircon age; Kozakov et al., 1993), 780 ± 20 Ma and 816
93 ± 13 Ma at Greater Karatau (multigrain zircon age; Kozakov et al., 1993; Pradhan, personal
94 communication), 771 ± 17 Ma for Talas (Pradhan, personal communication) and ages ranging
95 from 690-720 Ma for Dyzhetym Group in Kyrgyzstan (see Chumakov, 2009a). These younger
96 ages do not preclude older rocks being present in the basement of these domains.

97 The Neoproterozoic felsic and bi-modal volcanic series of several microcontinents are
98 argued to be coeval and are typically correlated with each other (Chumakov, 2009; Meert et al,
99 in press). Given the age data cited above these correlations seem reasonable. (Degtyarev and
100 Ryazantsev, 2007).

101 From ~750 Ma to ~550 Ma, the geologic record for most microcontinents of the
102 Kazakhstan domain is fragmented. Sedimentary rocks overlie the basement and late
103 Neoproterozoic volcanics on some microcontinents, for instance on the Ulutau microcontinent

104 (Knipper, 1963), but ages are usually inferred on general grounds and often vary from
105 publication to publication. In general, there appears to exist a regional ~100-200 Ma long hiatus,
106 approximately until Ediacaran - Nemakit-Daldynian time (Korolev and Maksumova, 1984;
107 Meert et al., in press).

108 The geological correlation between microcontinents improves in the terminal
109 Neoproterozoic. The thick carbonate-clastic sequences of latest Neoproterozoic to early
110 Paleozoic age are known on many CAOB microcontinents (Khain et al., 2003 and references
111 therein). The examples include the Karal and Basagin Fms. of the Aktau-Junggar massif and the
112 Tamdy Series of the Lesser Karatau in Kazakhstan. These carbonate-clastic sequences show
113 striking similarities (Ankinovich, 1961; Zubtsov, 1971). The most notable marker horizons are
114 late Neoproterozoic glacial diamictites that are known at one or more stratigraphic levels on
115 several microcontinents (Chumakov, 1978; Chumakov, 2009a; Korolev and Maksumova, 1984)
116 and phosphorite layers that occur at the Ediacaran – Cambrian boundary on some of these blocks
117 (Korolev and Maksumova, 1984; Meert and Lieberman, 2008; Meert et al., in press). Overall the
118 stratigraphic, faunal and lithological similarities led many authors to hypothesize that these
119 blocks originally constituted a continent-size “Kazakhstan” domain (Fig. 1b) with a
120 Paleoproterozoic basement and latest Neoproterozoic to early Paleozoic sedimentary cover (e.g.,
121 Degtyarev and Ryazantsev, 2007 and references therein).

122 Several microcontinents to the south of the Siberian platform (Fig. 1b) can be regarded as
123 remnants of a larger “Mongol” domain, that may have included the Baydaric and Tarbagatay
124 blocks, Tuva-Mongol composite massif (at least the Gargan block), and possibly several smaller
125 blocks. There are several lines of evidence that support a common origin for the Baydaric and
126 Tarbagatay blocks and the Tuva-Mongol massif:

- 127 1. The basement formation of the Tuva-Mongol composite massif was completed in the
128 Neoproterozoic with the accretion of continental (Gargan block), oceanic, and island-arc
129 terranes (Kuzmichev, 1996; 2004).
- 130 2. The crystalline basement is of similar age in the Baydaric and Tarbagatay blocks ($2646 \pm$
131 45 Ma, U-Pb on zircon, Kozakov et al., 1993) and in the Gargan block (2450 Ma, U-Pb on
132 zircons, Khain et al., 1995).
- 133 3. The last episode of pro-grade metamorphism occurred at 1800-1850 Ma in all these units
134 (Khain et al., 2003).
- 135 4. The late Neoproterozoic subduction-related Darkhat-Sarkhoy volcanic series of the Tuva-
136 Mongol massif is similar in age and composition to the Dzabkhan volcanic series of the
137 Baydaric block (Konnikov et al., 1994).

138 5. Finally, the carbonate-clastic covers of these blocks, (e.g. the Khubsugul Group of the
139 Tuva-Mongol massif and the Tsagan-Oloom Formation of the Baydaric block) that
140 accumulated in a passive-margin environment are similar (Belichenko et al, 1999) and
141 limited paleomagnetic data from these sequences supports the correlation (Kravchinsky et
142 al., 2001; 2010).

143 Hence we conclude that the Baydaric and Tarbagatay blocks and the Tuva-Mongol massif
144 are likely to have belonged to the same “Mongol” domain and therefore moved as a single plate
145 in the Precambrian.

146 3. Geological setting and sampling

147 Our study concentrated on the Lesser Karatau microcontinent in southern Kazakhstan
148 (Figs. 1b and 2). The most ancient rocks are exposed in a narrow band in the southwestern part
149 of the Lesser Karatau Range (Fig. 2) and consist of thick clastic flysch of the Bolshekaroy Series
150 (Fig. 3). Both series are of presumed Paleoproterozoic age (Sovetov, 1990). However, all
151 contacts are tectonic, and their temporal relationship is uncertain.

152 The late Neoproterozoic–early Paleozoic sedimentary cover overlies the basement with an
153 angular unconformity and most probably with a large hiatus (Sovetov, 1990). The cover is
154 exposed in a series of NW-striking thrust sheets (Fig. 2). The sedimentary cover is divided into
155 two series (Sovetov, 1990). The older Malokaroy Series is further divided into four formations
156 with conformable contacts between them: a) redbeds and conglomerates of the Koksuy Fm.; b)
157 arkoses and gritstones of the Aktugay Fm.; c) black mudstones and cherts of the Chichkan Fm.;
158 d) volcano-sedimentary rocks of the Kurgan Fm (Fig. 3).

159 The rocks of the Malokaroy Series are overlain, with stratigraphic and, locally, weak
160 angular unconformity by the mostly carbonate Tamdy Series which is further divided into
161 several formations (Fig. 3) (Eganov and Sovetov, 1979). The lowermost Kyrshabakty Fm. is
162 represented by a tilloid layer, overlain by pink dolomites, that are, in turn, overlain by a
163 carbonate – terrigenous member (Eganov and Sovetov, 1979). The carbonate Berkuty member of
164 the Chuluctau Fm. overlies the rocks of the Kyrshabakty Fm. with an erosional hiatus. Small
165 shelly fossils (*Protohertzina anabarica* Miss., *Unguliformis* Miss.) from the Berkuty member
166 correspond to the very end of Nemakit-Daldynian time (zone *Purella antiqua* ; Khomentovsky et
167 al., 1998). The carbonates of the Berkuty member are overlain by a phosphorite horizon of the
168 Tommotian age (Missargevsky and Mambetov, 1981) which is, in turn, covered by thick
169 Atdabanian to Middle Ordovician carbonates (Fig. 3) (Mambetov and Repina, 1979; Eganov and
170 Sovetov, 1979). The age of the lowermost Kyrshabakty Fm. remains uncertain. Eganov and
171 Sovetov (1979) assigned a Nemakit-Daldynian age to these rocks; however, the presence of

172 tillites suggests an older Ediacaran age (580 Ma, eg, Gaskiers) or more probably a Marinoan age
173 (~635 Ma; Meert et al., in press).

174 Our study concentrated on late Neoproterozoic volcano-sedimentary rocks of the Kurgan
175 Formation that are represented by interlayered pink, red, and green sandstones and siltstones
176 along with silicic tuffs (Fig. 3). The silicic volcanic rocks are mainly ash tuffs and massive
177 pyroclastic flows.

178 **4. U-Pb geochronology**

179 Two samples, K2006-2 and K2006-4, were collected for U-Pb geochronology from a
180 rhyolite tuff sequence at two levels within the Neoproterozoic Kurgan Fm (Fig. 3).

181 *4.1. Methods*

182 Zircons were extracted from K2006-2 and K2006-4 using standard mechanical crushing,
183 density, and magnetic separation techniques. The least magnetic zircons were then hand-picked
184 under a binocular scope, mounted in epoxy with the external zircon standard FC-1, and polished
185 to expose the zircons. U-Pb isotopic data were obtained from the zircons at the University of
186 Florida using laser ablation multi-collector inductively coupled plasma mass spectrometry (LA-
187 MC-ICP-MS). A New Wave 213 nm ultraviolet laser coupled with a Nu Plasma multi-collector
188 plasma source mass spectrometer was used to ablate individual zircons and to obtain U/Pb
189 isotopic abundances. The LA-MC-ICP-MS analytical equipment and procedure used in this
190 study are described by Simonetti et al. (2005).

191 The raw U-Pb isotopic ratios obtained from the K2006-2 and K2006-4 zircons by LA-MC-
192 ICP-MS were corrected for laser-induced elemental fractionation and instrumental drift as
193 outlined by Kosler and Sylvester (2003). The analytical errors from the individual zircon
194 unknown and FC-1 standard zircon analyses and true external standard values (TIMS data, Paces
195 and Miller, 1993) were then propagated quadratically for each analysis as described by
196 Horstwood et al. (2003). $^{206}\text{Pb}/^{238}\text{U}$ ratios were then corrected for common Pb using the “207
197 method” as summarized by Williams (1998). Common Pb corrected $^{207}\text{Pb}/^{235}\text{U}$ ratios were then
198 derived from known $^{238}\text{U}/^{235}\text{U}$ (137.88), the common Pb corrected $^{206}\text{Pb}/^{238}\text{U}$ ratios, and drift
199 corrected $^{207}\text{Pb}/^{206}\text{Pb}$ ratios. Conventional concordia diagrams were constructed for these data
200 using the Microsoft Excel spreadsheet add-in program Isoplot v. 3.09a by Ludwig (2004).

201 *4.2. Results*

202 U-Pb geochronology from samples K2006-2 and K2006-4 reveals both Paleoproterozoic-
203 Archean and Neoproterozoic zircons in the Kurgan rhyolite tuff sequence (Fig 4, Table 1).
204 K2006-2, collected near the base of the tuff sequence, yielded a population of small (~ 50-100
205 μm) subhedral zircons that yielded slightly discordant $^{206}\text{Pb}/^{238}\text{U}$ and $^{207}\text{Pb}/^{235}\text{U}$ ages ranging
206 from ~ 2039 to 2790 Ma. Twelve of these zircons are very similar in age and correspond to

207 concordia age of 2032 ± 14 Ma (2σ error). K2006-2 also yielded a population of larger (~ 150 -
208 $400 \mu\text{m}$) subhedral to euhedral zircons. All seven zircons from the larger population are similar
209 in age and gave a concordia age of 831 ± 15 Ma (2σ error, Fig. 4a). K2006-4, collected from
210 near the middle portion of the rhyolite tuff sequence, yielded a single population of small (~ 100 -
211 $200 \mu\text{m}$) euhedral zircons. Eight of the nine zircons analyzed from K2006-4 are concordant and
212 gave a concordia age of 766 ± 7 Ma (2σ , Fig. 4b).

213 The age of the tuff sequence at Lesser Karatau is most likely closer to the younger
214 concordia age of 766 ± 7 Ma. Although the 831 Ma age is concordant, the sample is best
215 described as a reworked tuff and therefore these zircons may be detrital or xenocrystic. The
216 Greater Karatau and Aktau-Mointy blocks contain zircons ranging between 816 - 880 Ma (see
217 Meert et al., in press) and represent a potential source region. Additional support for a ~ 770 Ma
218 age comes from ages obtained in the Talas Range---considered a stratigraphic equivalent of
219 Lesser Karatau-- of 771 ± 17 Ma (Pradhan, personal communication) and an age of 771 ± 17 Ma
220 for the Kurgan tuffs reported by Sovetov et al., (2008).

221 **5. Paleomagnetic study**

222 *5.1. Sampling*

223 The Kurgan Fm. outcrops in the lower parts of many thrust sheets in the Lesser Karatau
224 and dips to the north at various angles (Fig. 2). It is often poorly exposed, affected by penetrative
225 deformation and/or altered. Our sampling concentrated on the Shabakty section (A, $43^{\circ}30'N$,
226 $69^{\circ}52'E$; Fig. 2) where the Kurgan Fm. dips to the north, is nearly continuously exposed and
227 shows no signs of penetrative deformation. These same rocks, with different southeastern and
228 gentle dips, were found at one additional locality (B, $43^{\circ}33'N$, $69^{\circ}48'E$, Fig. 2). In total, we
229 sampled 35 sites from the red sandstones, siltstones, ash tuffs and massive pyroclastic flows
230 from two nearly monoclinical sections with distinctly different bedding attitudes.

231 Conglomerate beds are abundant in the Neoproterozoic section but always occur below the
232 Kurgan rocks. Nearly all debris in these conglomerates is represented by white quartz and
233 granite. The Kurgan Fm. includes several gritstone members with millimeter-sized debris of the
234 same composition as in the conglomerates below. The only place where greenish-gray cobbles of
235 the Kurgan rocks were found is a limited exposure of tillites of presumed Late Cryogenian age
236 in another thrust sheet to the north of the main section (C in Fig. 2; Meert et al., in press). The
237 Kurgan host rocks at that locality show strong schistosity, but the younger rocks, including the
238 tillite bed as well as the overlying dolomite, are not visibly affected, and we sampled 13 cobbles
239 of the Kurgan tuff from the tillites.

240 *5.2. Methods*

241 A set of samples collected from a one to three meters thick bed or several thinner beds over
242 a similar thickness interval was treated as a single site. The Kurgan rocks proved to be too hard
243 and fragile to permit efficient drilling, and paleomagnetic samples were therefore collected as
244 fist-sized blocks oriented with a magnetic compass. Our convention is to label a site using the
245 letters/numbers of its first sample but with a capital letter at the beginning; for instance, site
246 N4379 contains samples n4379 through to n4386, followed by site N4387, and so forth.

247 Cubic specimens of 8-cm³ volume were sawed from the hand samples. The collection was
248 studied in the Paleomagnetic Laboratory of the Geological Institute of the Russian Academy of
249 Sciences in Moscow. Specimens were heated in a homemade oven with internal residual fields of
250 approximately 10 nT and measured with a JR-4 spinner magnetometer with a noise level of 0.05
251 mA/m. The specimens were stepwise demagnetized in 15-20 increments up to 680°C.

252 Demagnetization results were plotted in orthogonal vector diagrams (Zijderveld, 1967).
253 Visually identified linear trajectories were used to determine directions of magnetic components
254 by Principal Component Analysis (PCA), employing a least-square fit comprising three or more
255 demagnetization steps (Kirschvink, 1980) and anchoring the fitting lines to the origin where
256 appropriate. If complete component separation is not achieved during demagnetization, the
257 common practice is to combine the PCA-calculated sample directions (Kirschvink, 1980) and
258 remagnetization circles for computing site-means of both lower- and higher-temperature
259 components, employing the technique of McFadden and McElhinny (1988).

260 Paleomagnetic software written by Jean-Pascal Cogné (2003), Randy Enkin
261 (http://gsc.nrcan.gc.ca/dir/index_e.php?id=12377), and Stanislav V. Shipunov was used in the
262 analysis.

263 5.3. Results

264 Intensity of the natural remanent magnetization (NRM) of the Kurgan rocks varies from
265 less than 1 mA/m to > 100 mA/m. A low-temperature component (LTC) was removed below
266 200° to 300° C from most samples.. The overall mean of this *in-situ* component ($D = 11.1^\circ$, $I =$
267 62.9° , $\alpha_{95} = 6.1^\circ$) is indistinguishable from the present-day field direction for the area ($D = 6^\circ$, $I =$
268 62°).

269 After removal of the present-day field overprint, three distinct demagnetization patterns are
270 observed, sometimes within a site. In some samples, a single component that does not decay to
271 the origin prevails over a temperature interval of up to 570° C, sometimes to 620-640° C (Fig.
272 5a). In a few cases, one intermediate-temperature component (ITC) was succeeded by another
273 that also did not decay to the origin (Fig. 5b); these remanences are labeled as ITC-1 and ITC-2
274 if both can be identified in a sample. More common are samples where an ITC is followed by a

275 component that shows rectilinear decay to the origin (Fig. 5c-e). This high-temperature
276 component (HTC) is usually resolved above $>570^{\circ}\text{C}$ or in other cases above 640°C .

277 In situ ITC site-means have similar southwesterly declinations, but inclinations vary from
278 moderately steep-and-up to shallow-and-down values, thus resulting in strongly elongated
279 distribution of the data from both fold limbs (Fig. 6a). Upon tilt correction, the scatter increases
280 (Fig. 6b; Table 2). At some sites, strongly elongated distributions of ITC directions were also
281 observed (Fig. 6c-d), whereas unblocking temperatures do not vary from sample to sample. Two
282 limb-mean ITC directions are statistically identical in geographic coordinates and are different
283 after tilt correction (Table 2), and the ITC therefore appears to be a post-folding component
284 (McFadden and Jones, 1981). It is argued that, for the late Paleozoic, the Baltica apparent polar
285 APWP (Torsvik and Cocks, 2005) can serve as a good reference for paleolatitudes for most
286 central Asia, although declinations are often rotated in both senses (Van der Voo et al., 2006). In
287 particular, a characteristic remanence in Upper Permian redbeds from the northern slopes of the
288 Lesser Karatau Range was deflected counterclockwise by $\sim 20^{\circ}$ with respect to the Baltica grid
289 (Bazhenov et al., 1995). Applying this same rotation to ITC component brings the ITC directions
290 closer to the reference direction (Fig. 6a).

291 In some samples, two different ITC components are recognized. These were identified
292 only at sites N4305 and N4363 (Table 2). The strongly elongated distributions at both area and
293 site levels (Fig. 6a, c-d) require an explanation. The ITC directions are more scattered (Table 2)
294 than typical overprint data that tend to be more tightly grouped. One possibility is that the
295 Kurgan rocks have just one ITC with southwest and up directions and the HTC, whereas the
296 directions with southwesterly declinations and shallow inclinations resulted from strong
297 overlapping of unblocking spectra of these two components. The fact that the HTC falls along a
298 great circle connected to the ITC data supports this hypothesis.

299 Another possibility is that there are two distinct remagnetization components present in the
300 Kurgan rocks. One is likely to be of (late?) Permian age and is the end-member of the observed
301 elongated distribution (Fig. 6a). The second is more problematic, but potentially may be of late
302 Ordovician age for the following reasons. The the main folding and thrusting in the Lesser
303 Karatau Range took place in the late Ordovician (Alexeiev, 1990; 1993), and there are coeval
304 granite intrusions in this area. Late Ordovician paleomagnetic results from the western
305 termination of the Tien Shan about one hundred kilometers to the northeast of our study area
306 generally have northward declinations and shallow negative inclinations of 10° to 20° ; the north-
307 pointing directions were argued to be of normal polarity (Bazhenov et al., 2003). It is therefore
308 possible that an Ordovician overprint of reverse polarity is present in the Kurgan rocks (diamond
309 in Fig. 6a).

310 Unfortunately, apart from the limited number of samples and sites where these two
311 overprints can be resolved, there is no way to divide the elongated distribution into the
312 “Permian” and “Late Ordovician” segments (Fig. 6a). Moreover, we are confident that
313 unblocking spectra of different components do overlap in the collection. On the other hand, the
314 elongated distributions for each limb fully overlap *in-situ* and become more distorted and
315 dissimilar after tilt correction. We consider this as an indication that both components are post-
316 folding, consistent with geological data.

317 The HTC was isolated in many samples in a temperature range that is characteristic of
318 hematite (Fig. 5). In some cases, where unblocking spectra overlap, remagnetization circles were
319 used to isolate the HTC component. Both linear segments and great-circle intersections were
320 combined when computing site means (McFadden and McElhinny, 1988). Most HTC directions
321 are south and down (Fig. 5c-d) although there are a few NW and up directions in the collection
322 (Fig. 5e). At site M1085, both polarities were identified in the lower and upper parts of the
323 approximately two meter thick multi-layer exposure of red sandstones (Table 3). The dispersion
324 of the HTC significantly decreases upon tilt correction (Table 3; Fig. 7a-b), and the best
325 grouping of HTC directions is achieved upon 100% unfolding (Fig. 7c). Out of 17 site-means
326 with south-and-up directions, 14 form a nearly circular cluster, whereas the remaining three are
327 shifted towards the overall ITC mean (gray triangles and inverted triangle, respectively, in Fig.
328 7b). We suspect that complete component separation was not achieved at these three sites, and
329 they are therefore excluded from the statistical analysis. Limb-mean HTC directions are
330 statistically different *in situ* and cluster after tilt correction (Table 3; Fig. 7d-e), supporting a pre-
331 folding remanence (McFadden and Jones, 1981). Hence this component predates all deformation
332 that has affected the Kurgan Fm and may be regarded as primary. The mean HTC inclination of
333 $53.7^\circ \pm 5.4^\circ$ corresponds to a paleolatitude of $34.2^\circ + 5.3^\circ$, N or S.

334 Most HTC site-mean directions point south and downward and form a tight cluster,
335 whereas some HTC vectors point northwest and upward at four sites (Table 3; Fig. 7a-b). Site-
336 means of *each polarity* are also better grouped after tilt-correction (Table 3), thus rendering the
337 fold test positive for each polarity (McElhinny, 1964). The two polarity-means differ by $\sim 160^\circ$,
338 and the critical angle γ_c of $\sim 10^\circ$ renders the reversal test negative (McFadden and McElhinny,
339 1990). The imperfect antipodality may be due to the limited number of north-and-up pointing
340 vectors or due to the incomplete removal of secondary postfolding components. We suggest that
341 both factors contribute to the observed pattern and that the presence of a dual-polarity pre-
342 folding magnetization is a strong indication of a primary remanence in the rocks.

343 The magnetization components in the cobbles are similarly complex. After removal of the
344 LTC, a single component that does not decay to the origin prevails in most cobbles (Fig. 5f). Its

345 mean *in-situ* direction- falls close to some ITC site-means (Table 2). This remanence clearly fails
346 the conglomerate test and is likely to be a late Paleozoic overprint. Another component with
347 higher unblocking temperatures was observed in many cobbles, but a clear isolation of this
348 remanence was possible in only five of the thirteen samples collected (Fig. 5g). The normalized
349 vector-resultant of 0.319 is less than the 95% critical value of 0.7 of the uniformity test (Mardia,
350 1972), and these five directions are chaotic. Due to the small number of vectors isolated in the
351 cobbles, we cannot confidently conclude a positive conglomerate test, but we argue that the
352 evidence further supports our claim of a primary remanence in the Kurgan Formation.

353 Paleomagnetic results are summarized as follows. A post-folding LTC of recent age is
354 common.. The ITC may be a mixture of two remanences (Permian overprint and the HTC), or a
355 late Ordovician component may be present as well. Irrespective of this ambiguity, the ITC is
356 post-folding and therefore post-dates the Late Ordovician. As noted above, main folding of the
357 Kurgan rocks occurred in the Late Ordovician, although an angular unconformity is observed
358 between the Kurgan Fm. and Ediacaran strata. The late Ordovician directions from the same
359 region are distinct from the HTC data (Figs. 6a and 7b). The south-and-up directions prevail in
360 the HTC data but at least two reversals are stratigraphically bound. Considering all of the
361 paleomagnetic evidence, we suggest that the HTC in the Kurgan rocks is older than the late
362 Ordovician and is likely to be primary in origin.

363 Reliable Neoproterozoic paleomagnetic data are available only for two of the CAOBS
364 microcontinents which are the Baydaric microcontinent in central Mongolia (part of the Mongol
365 domain, Levashova et al., 2010) and the Lesser Karatau microcontinent in Kazakhstan (part of
366 the Kazakhstan domain, this study; Fig. 1b). In the Baydaric microcontinent, Levashova et al.
367 (2010) reported a paleolatitude of $47^\circ \pm 14^\circ$, N or S, for Neoproterozoic (~770-800 Ma) volcanic
368 rocks of the Dzabkhan Fm. According to our new data, the volcano-sedimentary Kurgan Fm, that
369 is the upper member of the late Neoproterozoic cover of the Lesser Karatau block, accumulated
370 at a paleolatitude of $34.2^\circ \pm 5.3^\circ$, N or S, at about 766 ± 7 Ma.

371

372 **6. Interpretation and discussion**

373 Two new paleomagnetic results with ages of ~775 Ma from South Kazakhstan and from
374 Central Mongolia (Levashova et al., 2010) were obtained. The paleolatitudes of the Lesser
375 Karatau and the Baydaric microcontinents at about 775 Ma by themselves do not give an
376 opportunity to fix these two crustal fragments into a large-scale puzzle. As we are still eager to
377 consider our data on a broader scale, we have to combine the paleomagnetic data with the
378 tectonostratigraphic correlations between the CAOBS microcontinents and major cratons.

379 The tectonostratigraphic correlations between the CAOB microcontinents were discussed
380 earlier along with the observation that many of these microcontinents are floored by Precambrian
381 basement as old as Paleoproterozoic (including zircons recovered in the reworked tuff in our
382 study). This overall similarity allows us to conjecture that most CAOB microcontinents
383 originally belonged to two Madagascar-sized landmasses, the Kazakhstan and Mongol domains.

384 Most authors accept (or at least, tolerate) the existence of the Precambrian supercontinent
385 Rodinia that supposedly formed at ca. 1100 Ma and broke apart between 800 and 700 Ma (Meert
386 and Torsvik, 2003; Li et al., 2008, and references therein). The period from 800 Ma to about 540
387 Ma was a time of a major tectonic re-organization - the breakup of Rodinia, followed by the
388 formation of Gondwana (Meert, 2003; Meert and Torsvik, 2004; Meert and Lieberman, 2008).
389 For instance, Hoffman (1991) suggested that the break-up of Rodinia at about 800-700 Ma
390 involved fragmentation around Laurentia with continental fragments moving away from
391 Laurentia and colliding on the other side of the Earth to form Gondwana. Meert (2003) argued
392 that West Gondwana was largely assembled by ca. 600 Ma (with the exception of Kalahari and
393 perhaps some minor terranes), whereas Australia-East Antarctica, India, eastern Africa and
394 Kalahari were still separated by the oceanic basins (see also Gregory et al., 2009). Gondwana
395 was finally amalgamated by ca. 540-530 through the docking of India to Australia-East
396 Antarctica (Meert, 2003). However, due to the scarcity of paleomagnetic data, more accurate
397 kinematics of this sequence of events are poorly defined. Moreover, the orientation and location
398 of the landmasses that comprised Rodinia remain highly controversial (Meert and Torsvik,
399 2003), and it is thus premature to compare data from the Kazakhstan and Mongol domains with
400 different models of Rodinia.

401 As an alternative to a Rodinia comparison, we prefer to compare the observed
402 paleolatitudes from the Kazakhstan and Mongol domains to those recalculated from 750-800 Ma
403 paleomagnetic poles for other larger cratons. Note that neither paleomagnetic poles nor
404 declinations can be used for the Mongol and Kazakhstan regions because subsequent rotations
405 within the mobile CAOB have distorted them “beyond recognition”. Moreover, because of the
406 hemispheric ambiguity of paleomagnetic data, we have to examine both polarity options.

407 If the southern hemisphere option is chosen (downward-and-south pointing directions in
408 Fig. 7 are reverse), the Kazakhstan and Mongol domains are placed at mid-southern latitudes in
409 the vicinity of western Gondwana cratons (West Africa and Amazonia) or amidst the Brasiliano
410 Ocean. If we adhere to the northern hemisphere option (downward-and-south pointing directions
411 in Fig. 7 are normal), the paleolatitudes of these microcontinents are compatible with those for
412 Australia, Tarim, South China, India, and North China, whereas Siberia and Laurentia occupied
413 lower latitudes (Fig. 8, Table 4). The data scarcity for both microcontinents and cratons does not

414 permit a more definitive choice, and further progress requires a review of tectonostratigraphic
415 correlations between the CAOB microcontinents and major cratons.

416 The Neoproterozoic to early Paleozoic sections of the CAOB microcontinents show many
417 similarities not only with each other but also with coeval sections on the margins of Tarim,
418 Australia, South China, and, to a lesser degree, Siberia and North China (Korolev and
419 Maksumova, 1984; Esakova and Zhegallo, 1996; Khomentovsky, 1996; Li et al., 2002; Khain et
420 al., 2003; Xiao et al., 2004; Chumakov, 2009b). The geological arguments for these correlations
421 are: (1) The cratons have Archean to Paleoproterozoic basement; (2) Volcanic series that are
422 broadly coeval with the Neoproterozoic volcanic series of the CAOB microcontinents are known
423 in South China, Tarim and Australia; (3) The cratons have the late Neoproterozoic – Cambrian
424 carbonate – clastic sedimentary cover that show striking stratigraphic similarities to the
425 sedimentary cover of the microcontinents; (4) Late Neoproterozoic glacial deposits at one or
426 more stratigraphic levels are found on all of these cratons (Meert et al, in press; Chumakov,
427 2009a).

428 On the South China craton, rift-related bimodal magmatism was described at 830-795 Ma
429 and 780-745 Ma (Li et al., 2002). The late Neoproterozoic–Cambrian carbonate-clastic
430 sequences of the Yangtze area show striking similarities to the sedimentary cover of the CAOB
431 microcontinents, in particular to the Baydaric and Tuva-Mongol blocks in the Mongol domain,
432 and have up to three Neoproterozoic glacial intervals (Khomentovsky, 1996).

433 Probably best documented are the correlations between the Kazakhstan microcontinents
434 and the Tarim craton where detailed descriptions can be found (eg., Chumakov, 2009b). Here,
435 we mention that (1) the 820-750 Ma bimodal volcanic rocks in Tarim (Lu et al., 2008) may
436 correlate with the Neoproterozoic felsic and bi-modal volcanic series of many CAOB
437 microcontinents; (2) the late Neoproterozoic – Cambrian carbonate-clastic sequence of the
438 Quruqtagh range on Tarim is similar to coeval sections of the Kazakhstan domain and has up to
439 three Neoproterozoic glacial intervals (Xiao et al., 2004; Chumakov, 2009b). The above
440 evidence allowed Khain et al. (2003) to propose that a single Kazakhstan-Tarim continent
441 existed in the Neoproterozoic – Cambrian.

442 The Neoproterozoic to early Paleozoic sections of northwestern Australia also show some
443 similarities with the coeval CAOB sections. However, Chumakov (2009b) considers
444 stratigraphic similarities between the Australian sections and those of the CAOB microcontinents
445 to be less convincing. The Neoproterozoic volcanic series of the CAOB microcontinents are
446 broadly coeval the ca. 820–800 Ma lamprophyre dykes and kimberlite pipes in the Kimberley
447 craton of western Australia (Pidgeon et al., 1989) and the 755 Ma Mundine Well dyke swarm in
448 the northwestern Pilbara craton (Wingate and Giddings, 2000), but differ in character. The

449 Australian igneous activity is mafic/ultramafic whereas magmatism in the CAOB is more felsic
450 or bi-modal. While these differences may simply reflect distinct positions within the same
451 tectonic setting, we feel that they do not offer strong evidence of close affinity between the two
452 blocks. The sedimentary sections of the Kimberley region of northwestern Australia have up to
453 three Neoproterozoic glacial intervals (Li et al. 1996), but much of the remaining stratigraphy is
454 distinct from the CAOB sequences, but probably these facts do not give us enough ground for
455 the correlations with the CAOB microcontinents .

456 In North China, magmatic rocks ranging in age from 1100 to 700 Ma are rare (Zhao et al.,
457 2006; Lu et al., 2008). Late Neoproterozoic glacial diamictites are known here at more than one
458 stratigraphic level. The carbonate sequences of North China, however, can be correlated only
459 with the upper part of the sedimentary cover of Tarim, South China and the CAOB
460 microcontinents (Chumakov, 2009b).

461 We know of no studies where geological similarities between Neoproterozoic sections of
462 India and the CAOB microcontinents were proposed or validated, although depositional
463 sequences of the Krol-Tal Belt (Lesser Himalayas) might be a potential candidate for Late
464 Neoproterozoic-Cambrian comparison (Shanker et al., 2004) and the presence of a 750-800 Ma
465 large felsic igneous province in Rajasthan invites comparisons to the similarly-aged volcanic
466 sequences in the CAOB (Gregory et al., 2009; Meert et al., 2010; Pradhan et al., 2010).

467 It is possible to apply a combination of geologic and paleomagnetic “filters” in order to
468 identify potential ‘mother’ plate(s) for the CAOB blocks. We know of no geologic evidence of
469 connections between the CAOB microcontinents and future-West Gondwana cratons. Moreover,
470 extracting these microcontinents “from under Laurentia” and moving them through the future-
471 West Gondwana blocks requires an implausibly complicated trajectory to reach their Cambrian
472 configuration. Therefore, we reject a southern hemispheric origin for the CAOB
473 microcontinents.

474 We also note that irrespective of the polarity choice, Laurentia was positioned close to the
475 equator and shows few, if any, geologic similarities to be regarded as the mother-plate for the
476 CAOB microcontinents. Despite some geologic similarities between the CAOB microcontinents
477 and Siberia for the late Neoproterozoic interval, paleolatitudes for Siberia at 770 Ma are also too
478 low for placement adjacent to the CAOB and therefore we exclude Siberia from this list (Table
479 4, Fig. 8).

480 When examining the northern hemispheric option, India passes the paleomagnetic filter but
481 the geologic comparisons are not as strong, whereas the situation is reversed for the North China
482 craton. We propose that both can be excluded from the mother-plate list at the present time.
483 Finally, Australia passes the paleomagnetic filter, but there are the above-noted uncertainties in

484 stratigraphic correlations between Australia and the CAOB microcontinents (Chumakov, 2009b).

485 The above discussion essentially leaves us with two options, either Tarim and/or South
486 China, as potential mother plates for the Kazakhstan and Mongol domains. Either satisfies the
487 paleomagnetic similarity for coeval paleolatitudes and both show strong geological correlations.
488 Australia and India cannot be completely ruled out, but we consider them as less likely
489 candidates.

490 Available data are insufficient to establish the timing of the Kazakhstan and Mongol
491 domains separation from their mother-plate (plates?). However, the stratigraphic similarities
492 between the late Neoproterozoic – early Cambrian sedimentary covers of the above listed plates
493 and Kazakhstan and Mongol domains leaves us with two possibilities: (a) the domains did not
494 separate from their mother-plate (plates?) until the Early Cambrian; or (b) all these landmasses
495 were evolving under similar conditions in the late Neoproterozoic – early Cambrian.

496 Judged by the abundance of carbonates in the latest Neoproterozoic (ca. Ediacaran) –
497 Early Cambrian, all these units were located in a shallow and warm sea. In terminal
498 Neoproterozoic – Early Cambrian time, the paleomagnetic data for South China (Lin et al., 1985)
499 and available paleomagnetic results from the Tuva-Mongolia, Lesser Karatau and Baydaric
500 microcontinents (Kravchinsky et al., 2001, 2010; Pradhan et al., 2009) place the entire system at
501 equatorial latitudes.

502 A lithological and geochemical study of latest Neoproterozoic -Cambrian sedimentary
503 cover allowed Vescheva et al. (2008) to reconstruct the provenance of clastic material in
504 terrigenous rocks of the Tuva-Mongol massif. These authors concluded that plagioclase-
505 dominated granitoids of the Gargan block were the main suppliers, with a smaller contribution
506 from late Neoproterozoic ophiolites and island arc complexes. In contrast, a contribution from
507 the early Precambrian crust of the Siberian craton was nearly absent. Thus, according to
508 Vescheva et al. (2008), the Tuva-Mongol composite massif was neither welded to, nor proximal
509 to, Siberia. This conclusion is at directly at odds with recently published paleomagnetic data
510 from Eastern Sayan (Kravchinsky et al., 2010) that were used to place Tuva-Mongolia adjacent
511 to Siberia during the Cambrian.

512 In the Nemakit-Daldynian (ca. 542-530 Ma) and Tommotian (ca. 530-520 Ma), small
513 shelly fossils from the coeval sections of Tarim, South China, and the Aldan part of Siberia as
514 well as from several CAOB microcontinents have a number of similar taxa at the family, genus,
515 and even species levels (Esakova and Zhegallo, 1996). In the Atdabanian and Botomian (ca. 520-
516 512 Ma), Siberia, Tarim, South China, and the CAOB microcontinents belonged to the same
517 trilobite province and were distinct from Australia (Repina, 1985; Meert and Lieberman, 2004).
518 It is possible that trilobite spat were able to migrate between Siberia, Kazakzhstan, Tuva-

519 Mongol, Tarim and South China in a relatively small equatorial ocean bordering these
520 landmasses. The same is true for the first archaeocyathid reefs which had appeared in Siberia
521 within the humid tropical zone in the Tommotian and reached Australia somewhat later in the
522 middle of the Atdabanian (Zhuravleva, 1981; Meert and Lieberman, 2008). Repina (1985)
523 suggested that small shelly fossils migrated between these continents in a similar fashion.

524 Subduction-related complexes are recognized in different parts of the CAOB. For instance,
525 Ruzhentsev and Burashnikov (1995) described presumably Ediacaran - early Cambrian island
526 arc complexes in the Lake zone of western Mongolia and tentatively traced these island arcs to
527 the southeast of Tuva (Fig. 1b). The Selety island arc of Tommotian age in North Kazakhstan,
528 the 1000-km-long Bozshakol-Chingiz island arc in East Kazakhstan that originated in the
529 Atdabanian, and fragments of early Cambrian island arc complexes in South Kazakhstan
530 (Degtyarev and Ryazantsev, 2007) are most probably parts of the same puzzle. Unfortunately,
531 we cannot reconstruct the spatial relationship between the continental blocks and island arcs.
532 However, the lack of a tuffaceous influx in the carbonates suggests that the continental blocks
533 were likely distal from these now adjacent island arcs.

534 In an attempt to illustrate a much-generalized relationship between the cratons,
535 microcontinents and island arcs, we have drawn the above-discussed tectonic unit on a scheme
536 for the beginning of Cambrian time (Fig. 9) but must stress that this figure should not be
537 considered as a reconstruction (i.e., something certain and well defined). An oceanic domain was
538 probably located at equatorial latitudes to the north of Siberia. Following Chumakov (2009b),
539 we have positioned the Tarim craton adjacent to the Kazakhstan domain but shown the Tuva-
540 Mongol domain separately from either the South China or Tarim plates, in accord with the above
541 evidence.

542

543 7. Conclusions

544 We report new paleomagnetic data and U-Pb zircon ages for Neoproterozoic volcano-
545 sedimentary rocks from the Lesser Karatau block in central Kazakhstan. The LA-ICP-MS U-Pb
546 zircon age of felsic tuffs of the Kurgan Fm. is 766 ± 7 Ma. At that time the Lesser Karatau
547 microcontinent (central Kazakhstan) was located at a latitude of $34.2^\circ \pm 5.3^\circ$ N or S. The only
548 other CAOB microcontinent for which paleomagnetic data are available (at ~ 770 Ma) is the
549 Baydaric microcontinent in central Mongolia (Levashova et al., 2010). The LA-ICP-MS U-Pb
550 zircon age of volcanic rocks of the Dzabkhan Fm. is 770-805 Ma. At that time, the Baydaric
551 microcontinent was located at latitude of $47^\circ \pm 14^\circ$, N or S.

552 Several lines of evidence favor the view that CAOB microcontinents had originally been
553 parts of two larger domains and allow us to extrapolate the use of our paleomagnetic data to a

554 larger model of the Kazakhstan and Mongol domains. These domains may once have belonged
555 to major cratonic areas. Our combined analysis of paleomagnetic, geologic, geochronologic and
556 paleontologic data enabled us to exclude the southern hemisphere as a possible location of the
557 CAOB microcontinents at 750-800 Ma. Of several cratons that were located in the northern
558 hemisphere at that time we favor a hypothesis that the Kazakhstan and Mongol domains had
559 originally belonged either to Tarim or South China.

560 The available geological information indicates that a large, shallow, warm sea with an
561 archipelago of continental blocks existed to the north of Siberia in the end of the Neoproterozoic
562 – the beginning of the Paleozoic. We suggest that the Early Paleozoic “disposition” of the CAOB
563 units could resemble the present-day Arctic Canada archipelago but surrounded by multiple
564 subduction zones (Fig. 9).

565

566 **Acknowledgments**

567

568 We thank many colleagues from the Scientific Station of the Russian Academy of
569 Sciences in Bishkek (Kyrgyzstan) for logistic support of the fieldwork. We would like to thank
570 Kirill Degtyarev for helpful discussions and Alfred Kröner and an anonymous reviewer for
571 instructive comments. This study was supported by the Division of Earth Sciences and the Office
572 of International Science and Engineering's Eastern and Central Europe Program of the U.S.
573 National Science Foundation, grant EAR05-08597. Support was also derived from the Russian
574 Foundation of Basic Research, grant 07-05-00021, and Program no. 9 of the Earth Science
575 Division, Russian Academy of Sciences.

576

577 **References**

- 578 Alexeiev, D.V., 1990. The sequence of the Caledonian deformations in the Lesser Karatau
579 Ridge. *Geology and Ore prospecting in Kazakhstan, Alma-Ata*, 134-138, (in Russian).
- 580 Alexeiev, D.V., 1993. *Tectonics of the Lesser Karatau*. The PhD thesis, Moscow University,
581 Geological department, 145 p. (in Russian).
- 582 Ankinovich, S.G., 1962. The Lower Paleozoic of the vanadium-rich Central Tien-Shan Basin
583 and of the Central Kazakhstan west margin. *Alma-Ata*, 185 p. (in Russian).
- 584 Bazhenov, M.L., Klishevich, V.L., Tselmovich, V.A., 1995. Paleomagnetism of Permian red
585 beds from south Kazakhstan: DRM inclination error or CRM shallowed directions?
586 *Geophys. J. Int.* 120, 445-452.
- 587 Bazhenov, M.L., Collins, A.Q., Degtyarev, K.E., Levashova, N.M., Mikolaichuk, A.V., Pavlov,
588 V.E., Van der Voo, R., 2003. Paleozoic northward drift of the North Tien Shan (Central

- 589 Asia) as revealed by Ordovician and Carboniferous paleomagnetism. *Tectonophysics* 366,
590 113-141.
- 591 Belichenko, V.G., Letnikova, E.F., Geletii, N.K., 1999. Geology of Carbonate Rocks in the
592 Sedimentary Cover of the Tuva-Mongolia Microcontinent. *Doklady Earth Sci.* 364, 1-4.
- 593 Berzin, N.A., Dobretsov, N.L. 1994. Geodynamic evolution of Southern Siberia in Late
594 Precambrian - Early Paleozoic time. In: Coleman, R.G. (ed.), *Reconstruction of the*
595 *Paleoasian ocean*, Proc. 29th Intern Geol. Congr., Utrecht, VSP, 53-70
- 596 Burtman, V.S., 1999. Some problems of the Paleozoic tectonic reconstructions in Central Asia.
597 *Geotectonics* 33, 103-112.
- 598 Chen, Y., Xu, B., Zhan, S., Li, Y.G., 2004. First mid-Neoproterozoic paleomagnetic results from
599 the Tarim Basin (NW China) and their geodynamic implications. *Precambrian Res.* 133,
600 271–281.
- 601 Chumakov, N.M., 1978. *Precambrian tillites and tilloides*, Nauka, Moscow, 202 p. (in Russian).
- 602 Chumakov, N.M., 2009a. The Baykonurian glaciohorizon of the Late Vendian. *Stratigr. Geol.*
603 *Correl.* 17, 373-383.
- 604 Chumakov, N.M., 2009b. Neoproterozoic glacial events in Eurasia. In: Gaucher, C., Sial, A.N.,
605 Halverson, G.P., Frimmel, H.E. (Eds.), *Neoproterozoic – Cambrian Tectonics, Global*
606 *Change and Evolution: a focus on southwestern Gondwana*. *Developments in Precambrian*
607 *Geology*, 16, Elsevier, 389-403.
- 608 Cogné, J.P., 2003. PaleoMac: a Macintosh application for treating paleomagnetic data and
609 making plate reconstructions. *Geochem. Geophys. Geosyst.* 4(1), 1007,
610 doi:10.1029/2001GC000227 .
- 611 Degtyarev, K.E., Ryazantsev, A.V., 2007. Cambrian arc – continent collision in the Paleozooids
612 of Kazakhstan. *Geotectonics* 41, #1, 63-86
- 613 Didenko, A.N., Mossakovsky, A.A., Pechersky, D.M., Ruzhentsev, S.V., Samygin, S.G.,
614 Kheraskova, T.N., 1994. Geodynamics of Paleozoic oceans of Central Asia. *Russ. Geol.*
615 *Geophys. no. 7-8*, 59-75 (in Russian).
- 616 Eganov, E.A. and Y.K. Sovetov, 1979. The Karatau Range as a model of Phosphorite
617 accumulation. *Nauka, Novosibirsk*, 190 p. (in Russian)
- 618 Esakova, N.V., Zhegallo, E.A., 1996. The biostratigraphy and fauna of the Early Cambrian in
619 Mongolia. *Moscow, Nauka*, 270 p. (in Russian).
- 620 Evans, D.A., Zhuravlev, A.Y., Budney, C.J., Kirschvink, J.L., 1996. Palaeomagnetism of the
621 Bayan-Gol Formation, western Mongolia. *Geol. Mag.* 133, 487-496.

- 622 Evans, D.A.D., Li, Z.X., Kirschvink, J.L., Wingate, M.T.D., 2004. A high-quality mid-
623 Proterozoic paleomagnetic pole from South China, with implications for an Australia –
624 Laurentia connection at 755 Ma. *Precambrian Res.* 100, 213–234.
- 625 Fisher, R.A., 1953. Dispersion on a sphere. *Proc. R. Soc. London, Ser. A*, 217, 295-305.
- 626 Gregory, L.C., Meert, J.G., Bingen, B.H. Pandit, M.K., Torsvik, T.H., 2009. Paleomagnetic and
627 geochronologic study of Malani Ingeous suite, NW India: implications for the
628 configuration of Rodinia and the assembly of Gondwana. *Precambrian Res.* 170, 13-26.
- 629 Hargraves, R.B., Duncan, R.A., 1990. Radiometric age and paleomagnetic results from
630 Seychelles dikes. In: Duncan, R.A., et al. (Eds.), *Proceedings of the Ocean Drilling
631 Program. Scientific Results Leg*, vol. 115, pp. 119– 122.
- 632 Harlan, S.S., Geissman, J.W., Snee, L.W., 1997. Paleomagnetic and $^{40}\text{Ar}/^{39}\text{Ar}$ geochronologic
633 data from Late Proterozoic mafic dykes and sills, Montana and Wyoming. USGS
634 Professional Paper 1580, 16 pp.
- 635 Heaman, L.M., Le Cheminant, A.N., Rainbird, R.H., 1992. Nature and timing of Franklin
636 igneous events, Canada - implications for a late Proterozoic mantle plume and the break-up
637 of Laurentia. *Earth Planet. Sci. Lett.* 109, 117–131.
- 638 Hodych, J.P., Cox, R.A., Kořsler, J., 2004. An equatorial Laurentia at 550 Ma confirmed by
639 Grenvillian inherited zircons dated by LAM ICP-MS in the Skinner Cove volcanics of
640 western Newfoundland: implications for inertial interchange true polar wander.
641 *Precambrian Res.* 129, 93–113.
- 642 Hoffman, P.F., 1991. Did the breakout of Laurentia turn Gondwanaland inside-out? *Science* 252,
643 1409-1412.
- 644 Horstwood, M.S.A., Foster G.L., Parrish R.R., Noble S.R., Nowell G.M., 2003. Common-Pb
645 corrected in situ U-Pb accessory mineral geochronology by LA-MC-ICP-MS. *J. of
646 Analytical Atomic Spectrometry* 18, 837-846.
- 647 Huang, B.C., Xu, B., Zhang, C.X., Li, Y.A., Zhu, R.X., 2005. Paleomagnetism of the Baiyisi
648 volcanic rocks (ca.740 Ma) of Tarim Northwest China: a continental fragment of
649 Neoproterozoic Western Australia? *Precambrian Res.* 142, 83–92.
- 650 Iglesia-Llanos, M.P., Tait, J.A., Popov, V., Ablamasova, A., 2005, Paleomagnetic data from
651 Ediacaran (Vendian) sediments of the Arkhangelsk region, NW Russia: an alternative
652 APWP of Baltica for the Late Proterozoic – Early Paleozoic. *Earth Planet. Sci. Lett.* 240,
653 732-747.
- 654 Kamo, S.L., Gower, C.F., 1994. Note: U–Pb baddeleyite dating clarifies age of characteristic
655 paleomagnetic remanence of Long Range dykes, southeastern Labrador. *Atlantic Geol.* 30,
656 259–262.

- 657 Khain, E.V., Neimark, L.A., Amelin, U.V., 1995. Caledonian stage of remobilization of the
658 Gargan block basement, Eastern Sayan (isotopic geochronological data). *Doklady Earth*
659 *Sci.* 342, 776-780 (in Russian).
- 660 Khain, E.V., Bibikova, E.V., Salnikova, E.B., Kröner, A., Gibsher, A.S., Didenko, A.N.,
661 Degtyarev, K.E., Fedotova, A.A., 2003. The Palaeo-Asian ocean in the Neoproterozoic and
662 early Palaeozoic: new geochronologic data and palaeotectonic reconstructions.
663 *Precambrian Res.* 122, 329-358
- 664 Kheraskova, T.N., Didenko, A.N., Bush, V.A., Volozh, Y.A., 2003. The Vendian-Early
665 Paleozoic history of the continental margin of eastern Paleogondwana, Paleoasian Ocean,
666 and Central Asian Foldbelt, *Russ. J. Earth Sci.* 5, # 3, 165–184
- 667 Khomentovsky, V.V., 1996. The Sinian system of China and its analogies in Siberia. *Russ. Geol.*
668 *Geophys.* 37, no. 8, 136-153.
- 669 Khomentovsky, V.V., Fedorov, A.B., Karlova, G.A., 1998. The lower boundary of the Cambrian
670 in the inner regions of the northern part of the Siberian platform, *Stratigr. Geol. Correl.* 6,
671 no. 1, 3-11.
- 672 Kirschvink, J.L., 1978. The Precambrian Cambrian boundary problem; magnetostratigraphy of
673 the Amadeus Basin, central Australia. *Geol. Mag.* 115, 139– 150.
- 674 Kirschvink, J.L., 1980. The least-square line and plane and the analysis of palaeomagnetic data:
675 *Geophys. J. Roy. Astron. Soc.* 62, 699-718.
- 676 Knipper, A.L., 1963. Tectonics of the Baykonur Synclinorium (Central Kazakhstan). *Akademia*
677 *Nauk SSSR, Moscow*, 204 p. (in Russian).
- 678 Konnikov, E.G., Gibsher, A.S., Izokh, A.E., Skliarov, E.V., Khain, E.V., 1994. Late Precambrian
679 evolution of the Paleoasian ocean northern segment: new radiological, geological and
680 geochronological data. *Russ. Geol. Geophys.*, no. 7-8, 152-168 (in Russian).
- 681 Kosler, J., Sylvester, P.J., 2003. Present trends and the future of zircon in geochronology: Laser
682 ablation ICPMS, *Zircon. Reviews in Mineralogy and Geochemistry* 53, 243-271.
- 683 Korolev, V.G., Maksumova, R.A., 1984. Precambrian tillites and tilloides of the Tien-Shan. *Ilim,*
684 *Frunze*, 189 p. (in Russian).
- 685 Kozakov, I.K., Bibikova, E.V., Neymark, L.A., Kirnozova, T.I., 1993. The Baydaric block. In:
686 Rudnik, B.A., Sokolov, Y.M., Filatova, L.I. (Eds.), *Early Precambrian of the Central Asian*
687 *Fold Belt.* Nauka, St. Petersburg, 118-137 (in Russian).
- 688 Kravchinsky, V.A., Konstantinov, K.M., Cogné, J.-P., 2001. Paleomagnetic study of Vendian
689 and Early Cambrian rocks of South Siberia and Central Mongolia: was the Siberian
690 platform assembled at this time? *Precambrian Res.* 110, 61-92.

- 691 Kravchinsky, V.A., Sklyarov, E.V., Gladkochub, D.B., Harbert, W.P., 2010. Paleomagnetism
692 of the Precambrian Eastern Sayan rocks: Implications for the Ediacaran–Early Cambrian
693 paleogeography of the Tuva-Mongolian composite terrane. *Tectonophysics* 486, 65-80.
- 694 Kröner, A., Windley, B.F., Badarch, G., Tomurtogoo, O., Hegner, E., Jahn, B.M., Gruschka, S.,
695 Khain, E.V., Demoux, A., Wingate, M.T.D., 2007. Accretionary growth and crust
696 formation in the Central Asian Orogenic Belt and comparison with the Arabian-Nubian
697 shield. *Geol. Soc. Am. Mem.* 200, 181-209.
- 698 Kuzmichev, A.B., 1996. Riphean Ophiolites of the Kitoi Bald Mountains: Structural Setting and
699 Obduction Age. *Geologia i Razvedka* no. 3, 11-25 (in Russian).
- 700 Kuzmichev, A.B., 2004. Tectonic history of the Tuva-Mongol massif: Early Baikalian, Late
701 Baikalian and Early Caledonian stages. *PROBEL-2000*, Moscow, 192 p. (in Russian).
- 702 Levashova, N.M., Kalugin, V.M., Gibsher, A.S., Yff, J., Ryabinin, A.B., Meert, J.G., Malone,
703 S.J., 2010. The Origin of the Baydaric Microcontinent, Mongolia: Constraints from
704 Paleomagnetism and Geochronology. *Tectonophysics* 485, 306-320.
- 705 Li, X.H., Li, Z.X., Zhou, H., Liu, Y., Kinny, P.D., 2002. U-Pb zircon geochronology,
706 geochemistry and Nd isotopic study of Neoproterozoic bimodal volcanic rocks in the
707 Kangdian Rift of South China; implications for the initial rifting of Rodinia. *Precambrian*
708 *Res.* 113, 135-154.
- 709 Li, Z.X., Zhang, L., Powell, C.M., 1996. Positions of the East Asian cratons in the
710 Neoproterozoic supercontinent Rodinia. *Aust. J. Earth Sci.* 43, 593-604.
- 711 Li, Z.X., 2000. New palaeomagnetic results from the “cap dolomite” of the Neoproterozoic
712 Walsh Tillite, northwestern Australia. *Precambrian Res.* 100, 359–370.
- 713 Li, Z.X., Evans, D.A.D., Zhang, S., 2004. A 90° spin on Rodinia: possible causal links between
714 the Neoproterozoic supercontinent, superplume, true polar wander and low-latitude
715 glaciation. *Earth Planet. Sci. Lett.* 220, 409–421.
- 716 Li, Z.X., Bogdanova, S.V., Davidson, A., Collins, A.S., De Waele, B., Ernst, R.E., Fitzsimons,
717 I.C.W., Fuck, R.A., Gladkochub, D.P., Jacobs, J., Karlstrom, K.E., Lu, S., Natapov, L.M.,
718 Pease, V., Pisarevsky, S.A., Thrane, K., Vernikovsky, V., 2008. Assembly, configuration,
719 and break-up history of Rodinia: A synthesis. *Precambrian Res.* 160, 179-210.
- 720 Lin, J.L., Fuller, M.D., Zhang, W.Y., 1985. Paleogeography of the North and South China blocks
721 during the Cambrian. *J. Geodynamics* 2, 91– 114.
- 722 Lu, S., Zhao, G., Wang, H., Hao, G., 2008. Precambrian basement and sedimentary cover of the
723 North China Craton: A review. *Precambrian Res.* 160, 77-93.
- 724 Ludwig, K.R., 2004. Users manual for ISOPLOT, a geochemical toolkit for Microsoft Excel
725 version 3.09a.

- 726 Zhao, G.C., Cao, L., Wilde, S.A., Sun, M., Li, S.Z., 2006. Implications based on the first
727 SHRIMP U-Pb zircon dating on Precambrian granitoid rocks in North Korea. *Earth Planet.*
728 *Sci. Lett.* 251, 365-379.
- 729 Mambetov, A.M., Repina, L.N., 1979. The Lower Cambrian of the Talas Ala-too and its
730 correlation with the sections of the Lesser Karatau and the Siberian platform, in:
731 Zhuravleva, I.T., Meshkova, N.P., eds., *Biostratigraphy and paleontology of the Lower*
732 *Cambrian of the Siberian platform.* Nauka, Novosibirsk, 98-138 (in Russian).
- 733 Mardia, K.V., 1972. *Statistics of directional data.* Academic Press, London, 357 p.
- 734 McElhinny, M.W., 1964. Statistical significance of the fold test in palaeomagnetism. *Geophys. J.*
735 *Roy. Astron. Soc.* 8, 338-340.
- 736 McFadden, P.L., Jones, D.L., 1981. The fold test in palaeomagnetism. *Geophys. J. Roy. Astron.*
737 *Soc.* 67, 53-58
- 738 McFadden, P.L., and McElhinny, M.W., 1988. The combined analysis of remagnetization circles
739 and direct observations in palaeomagnetism. *Earth Planet. Sci. Lett.* 87, 161-172.
- 740 McFadden, P.L., McElhinny, M.W., 1990. Classification of the reversal test in palaeomagnetism.
741 *Geophys J. Int.* 103, 725-729
- 742 McWilliams, M.O., McElhinny, M.W., 1980. Late Precambrian paleomagnetism in Australia: the
743 Adelaide Geosyncline. *J. Geol.* 88, 1-26.
- 744 Meert, J.G., Van der Voo, R., Payne, T., 1994. Paleomagnetism of the Catoclin volcanic
745 province: a new Vendian-Cambrian apparent polar wander path for North America. *J.*
746 *Geophys. Res.* 99 (B3), 4625-4641.
- 747 Meert, J.G., Gibsher, A.S., Levashova, N.M., Grice, W.C., Kamenov, G.D. and Rybanin, A.,
748 2011. Glaciation and ~770 Ma Ediacaran (?) fossils from the Lesser Karatau
749 microcontinent, Kazakhstan, *Gondwana Res.*, in press.
- 750 Meert, J.G., Pandit, M.K., Pradhan, V.R., Banks, J., Sirianni, R., Stroud, M., Newstead, B. and
751 Gifford, J., 2010. Precambrian crustal evolution of Peninsular India: A 3.0 billion year
752 odyssey. *J. Asian Earth Sci.* 39, 483-515.
- 753 Meert, J.G., 2003. A synopsis of events related to the assembly of eastern Gondwana.
754 *Tectonophysics* 362, 1-40.
- 755 Meert, J.G., Torsvik, T.H., 2003. The making and unmaking of a supercontinent: Rodinia
756 revisited. *Tectonophysics* 375, 261-288.
- 757 Meert, J.G., Torsvik, T.H., 2004. Reply to J.D.A. Piper: The making and unmaking of a
758 supercontinent: Rodinia Revisited. *Tectonophysics* 383, 99-103.

- 759 Meert, J.G., Lieberman, B.S., 2004. A palaeomagnetic and palaeobiogeographical perspective on
760 latest Neoproterozoic and early Cambrian tectonic events, *J. Geol. Soc. Lond.* 161, 477-
761 487.
- 762 Meert, J.G., Lieberman, B.S., 2008. The Neoproterozoic assembly of Gondwana and its
763 relationship to the Ediacaran-Cambrian radiation. *Gondwana Res.* 14, 5-21.
- 764 Metelkin, D.V., Belonosov I.V., Gladkochub D.P., Donskaya T.V., Mazukabzov A.M.,
765 Stanevich, A.M., 2005. Paleomagnetic directions from Nersa intrusions of the Birusa
766 terrane, Siberian craton as a reflection of tectonic events in the Neoproterozoic. *Russ. Geol.*
767 *Geophys.* 46, 395-410 (in Russian).
- 768 Missargevsky, V.V., Mambetov, A.M., 1981. Stratigraphy and fauna of the boundary layers of
769 Cambrian and Precambrian in the Lesser Karatau. Nauka, Moscow, 92 p. (in Russian).
- 770 Mossakovsky, A.A., Ruzhentsev, S.V., Samygin, S.G., Kheraskova, T.N., 1993. The Central
771 Asian fold belt: Geodynamic evolution and formation. *Geotectonics* 27, no. 6, 3-32.
- 772 Murthy, G., Gower, C., Tubrett, M., Patzold, R., 1992. Paleomagnetism of Eocambrian Long
773 Range dykes and Double Mer Formation from Labrador Canada. *Can. J. Earth Sci.* 29,
774 1224–1234.
- 775 Paces, J. B., Miller, Jr., J.D., 1993. Precise U-Pb ages of Duluth complex and related mafic
776 intrusions, Northeastern Minnesota: Geochronological insights to physical, petrogenetic,
777 paleomagnetic, and tectonomagmatic processes associated with the 1.1 Ga midcontinent
778 rift system. *J. Geophys. Res.* 98, 13,997-14,013.
- 779 Palmer, H.C., Baragar, W.R.A., Fortier, M., Foster, J.H., 1983. Paleomagnetism of Late
780 Proterozoic rocks, Victoria Island, Northwest Territories, Canada. *Can. J. Earth Sci.* 20,
781 1456–1469.
- 782 Park, J.K., 1994. Palaeomagnetic constraints on the position of Laurentia from middle
783 Neoproterozoic to Early Cambrian times. *Precambrian Res.* 69, 95–112.
- 784 Park, J.K., Norris, D.K., Larochele, A., 1989. Paleomagnetism and the origin of the Mackenzie
785 Arc of northwestern Canada. *Can. J. Earth Sci.* 26, 2194–2203.
- 786 Pidgeon, R.T., Smith, C.B., Fanning, C.M., 1989. Kimberlite and lamproite emplacement ages in
787 Western Australia. In: Ross, J., et al. (Eds.), *Kimberlites and related rocks, Volume 1:*
788 *Their composition, Occurrence, Origin and Emplacement.* Blackwell Scientific
789 Publications, Carlton, pp.382-391 (Geol. Soc. Aust. Special Publication)
- 790 Pisarevsky, S.A., Wingate, M.T.D., Stevens, M.K., Haines, P.W., 2007. Paleomagnetic results
791 from the Lancer-1 stratigraphic drill hole, Officer Basin, Western Australia, and
792 implications for Rodinia reconstructions. *Aust. J. Earth Sci.* 54, 561–572.

- 793 Popov, V., Iosifidi, A., Khramov, A., Tait, J., Bachtadze, V., 2002. Paleomagnetism of Upper
794 Vendian sediments from the Winter Coast, White Sea region, Russia: implications for the
795 paleogeography of Baltica during Neoproterozoic times. *J. Geophys. Res.* 107, 2315.
- 796 Popov, V., Khramov, A., Bachtadze, V., 2005. Paleomagnetism, magnetic stratigraphy and
797 petromagnetism of the Upper Vendian sedimentary rocks in the sections of the Zolotitsa
798 River and in the Verkhotina Hole, Winter Coast of the White Sea, Russia. *Russ. J. Earth
799 Sci.* 7, 1-29.
- 800 Pradhan, V.R., Meert, J.G., Levashova, N.M. Gibsher, A.S., 2009. Preliminary paleomagnetic
801 data on Late Cambrian to Ordovician carbonate beds of Tamdy Series from the Lesser
802 Karatau microcontinent, South Kazakhstan. *Geological Soc. Am. abstracts* 41:7, 269.
- 803 Pradhan, V.R., Meert, J.G., Pandit, M.K., Kamenov, G., Gregory, L.C., Malone, S.J., 2008.
804 India's changing place in global Proterozoic reconstructions: New geochronologic
805 constraints on key paleomagnetic poles from the Dharwar and Aravalli/Bundelkhand
806 cratons. *J. Geodynamics* 50, 224-242.
- 807 Puchkov, V.N., 2000. Paleogeodynamics of the Southern and Middle Urals. Dauria, Ufa, 146 p.
808 (in Russian).
- 809 Repina, L.N., 1985. The Paleobiogeography of the Early Cambrian seas based on trilobites. In:
810 Khomentovsky, V.V. (ed.), *Biostratigraphy and Biogeography of the Paleozoic in Siberia.*
811 Academy of Sciences, Novosibirsk, 5-15 (in Russian).
- 812 Rui, Z.Q., Piper, J.D.A., 1997. Paleomagnetic study of Neoproterozoic glacial rocks of the
813 Yangtze Block; paleolatitudes and configuration of South China in the late Proterozoic
814 supercontinent. *Precambrian Res.* 85, 173-199.
- 815 Ruzhentsev, S.V., Burashnikov, V.V., 1995. The tectonics of the Western Mongolia Salairides.
816 *Geotectonics* 29, no. 5, 25-40.
- 817 Sengör, A.M.C., Natal'in, B.A., 1996. Paleotectonics of Asia: fragments of a synthesis. In: Yin,
818 A. et al. (eds.), *The tectonic evolution of Asia.* Cambridge University Press, Cambridge,
819 486-640.
- 820 Shanker, R., Bhattacharya, D.D., Pande, A.C., Mathur, V.K., 2004. Ediacaran biota from the
821 Jarashi (Middle Krol) and Mahi (Lower Krol) Formations, Krol Group, Lesser Himalaya,
822 India. *J. Geol. Soc. India* 63, 649-654.
- 823 Shatsillo, A.V., Didenko, A.N. Pavlov, V.E., 2006. Paleomagnetism of Vendian Deposits of the
824 Southwestern Siberian Platform. *Russ. J. Earth Sci.* 8, ES2003,
825 doi:10.2205/2005ES000182.

- 826 Simonetti, A., Heaman, L.M., Hartlaub, R.P., Creaser, R.A., MacHattie, T.G., Bohm, C., 2005.
827 U-Pb zircon dating by laser ablation-MC-ICP-MS using a new multiple ion counting
828 Faraday collector array. *J. of Analytical Atomic Spectroscopy* 20, 677-686.
- 829 Sohl, L.E., Christie-Blick, N., Kent, D.V., 1999. Paleomagnetic polarity reversals in Marinoan
830 (ca 600 Ma) glacial deposits of Australia: Implications for the duration of low-latitude
831 glaciation in Neoproterozoic time. *Geol. Soc. Am. Bull.* 111, 1120–1139.
- 832 Sovetov, Y.K., 1990. The Precambrian-Cambrian boundary and Precambrian sedimentary
833 assemblages in the Lesser Karatau : stratigraphic, sedimentologic and paleotectonic
834 aspects. Russian Academy of Sciences, Novosibirsk, Preprint #14, 36 p. (in Russian).
- 835 Stampfli, G.M., Borel, G.D., 2002. A plate tectonic model for the Paleozoic and Mesozoic
836 constrained by dynamic plate boundaries and restored synthetic oceanic isochrones. *Earth
837 Planet. Sci. Lett.* 196, 17-33.
- 838 Symons, D.T.A., Chiasson, A.D., 1991. Paleomagnetism of the Callander Complex and the
839 Cambrian apparent polar wander path for North America. *Can. J. Earth Sci.* 28, 355–363.
- 840 Tanczyk, E.I., Lapointe, P., Morris, W.A., Schmidt, P.W., 1987. A paleomagnetic study of the
841 layered mafic intrusions at Sept-Iles, Quebec. *Can. J. Earth Sci.* 24, 1431–1438.
- 842 Torsvik, T.H., Carter, L.M., Ashwal, L.D., Bhushan, S.K., Pandit, M.K., Jamtveit, B., 2001a.
843 Rodinia refined or obscured: palaeomagnetism of the Malani igneous suite (NW India).
844 *Precambrian Res.* 108, 319–333.
- 845 Torsvik, T.H., Ashwal, L.D., Tucker, R.D., Eide, E.A., 2001b. Neoproterozoic geochronology
846 and palaeogeography of the Seychelles microcontinent: the India link. *Precambrian Res.*
847 110, 47–59.
- 848 Torsvik, T.H., Rehnstrom, E.F., 2001. Cambrian paleomagnetic data from Baltica: implications
849 for true polar wander and Cambrian paleogeography. *J. Geol. Soc. Lond.* 158, 321– 329.
- 850 Torsvik, T.H., Cocks, L.R.M., 2005. Norway in space and time: A Centennial cavalcade.
851 *Norwegian Journal of Geology* 85, 73-86.
- 852 Van der Voo, R., Levashova, N.M., Skrinnik, L.S., Kara, T.V., Bazhenov, M.L., 2006. Late
853 orogenic, large-scale rotations in the Tien Shan and adjacent mobile belts in Kyrgyzstan
854 and Kazakhstan. *Tectonophysics* 426, 335-360.
- 855 Veshcheva, S.V., Turkina, O.M., Letnikova, E.F., Ronkin, Y.L., 2008. Geochemical and Sm-Nd
856 isotopic characteristics of the Neoproterozoic terrigenous rocks of the Tuva-Mongol
857 massif. *Doklady Earth Sciences* 418, 155-160.
- 858 Walderhaug, H.J., Torsvik, T.H., Eide, E.A., Sundvoll, B., Bingen, B., 1999. Geochronology and
859 paleomagnetism of the Hunnedalen dykes, SW Norway: implications for the
860 Sveconorwegian apparent polar wander loop. *Earth Planet. Sci. Lett.* 169, 71–83.

- 861 Walderhaug H. J., T. H. Torsvik, E. Halvorsen, 2007. Geomagnetism, rock magnetism and
862 palaeomagnetism. The Egersund dykes (SW Norway): a robust Early Ediacaran (Vendian)
863 palaeomagnetic pole from Baltica. *Geophys. J. Int.* 168, 935–948
- 864 Walter, M.R., Veevers, J.J., Calver, C.R., Gorjan, P., Hill, A.C., 2000. Dating the 840– 544 Ma
865 Neoproterozoic interval by isotopes of strontium, carbon and sulfur in seawater, and some
866 interpretative models. *Precambrian Res.* 100, 371– 432.
- 867 Weil, A.B., Geissman, J.W., Van der Voo, R., 2004. Paleomagnetism of the Neoproterozoic
868 Chuar Group, Grand Canyon Supergroup, Arizona: implications for Laurentia's
869 Neoproterozoic APWP and Rodinia break-up. *Precambrian Res.* 129, 71–92.
- 870 Williams, I.S., 1998. U-Th-Pb Geochronology by Ion Microprobe, in, McKibben, M.A., Shanks
871 III, W.C., Ridley, W.I., eds., *Applications of microanalytical techniques to understanding*
872 *mineralizing processes. Reviews in Economic Geology* 7, 1-35.
- 873 Windley, B.P., Alexeiev, D.V., Xiao, W., Kröner, A., Badarch, G., 2007. Tectonic models for
874 accretion of the Central Asian Orogenic Belt. *J. Geol. Soc. Lond.* 164, 31–47.
- 875 Wingate, M.T.D., Giddings, J.W., 2000. Age and paleomagnetism of the Mundine Well dyke
876 swarm, western Australia: implications for an Australia –Laurentia connection at 750 Ma.
877 *Precambrian Res.* 100, 335– 357.
- 878 Xiao, S.H., Bao, H.M., Wang, H.F., Kaufman, A.J., Zhou, C.M., Li, G.X., Yuan, X.L., Ling,
879 H.F., 2004. The Neoproterozoic Quruqtagh Group in eastern Chinese Tianshan: evidence
880 for a post-Marinoan glaciation. *Precambrian Res.* 130, 1-26.
- 881 Yakubchuk, A., Cole, A., Seltmann, R., Shatov, V.V., 2002. Tectonic setting, characteristics, and
882 regional exploration criteria for gold mineralization in the Altaid tectonic collage: the Tien
883 Shan province as a key example. *Society of Economic Geologists, Special Publications*, 9,
884 177-201.
- 885 Yakubchuk, A., 2008. Re-deciphering the tectonic jigsaw puzzle of northern Eurasia. *J. Asian*
886 *Earth Sci.* 32, 82-101.
- 887 Zhang, S., Li, Z.X., Wu, H., 2006. New Precambrian palaeomagnetic constraints on the position
888 of the North China Block in Rodinia. *Precambrian Res.* 144, 213–238.
- 889 Zhuravleva, I.T., 1981. Paleobiogeography of the Early Cambrian, *Paleontology,*
890 *paleobiogeography and plate tectonic concept, SVNIMS, Magadan*, 43-51 (in Russian).
- 891 Zonenshain, L.P., Kuzmin, M.I., Natapov, L.M., 1990. *Geology of the USSR: a plate-tectonic*
892 *synthesis. American Geophysical Union, Washington, D.C., Geodynamics Series* 21, 242
893 p.
- 894 Zijdeveld, J.D.A., 1967. AC demagnetization of rocks: analysis of results, In: Collinson, D.W.
895 et al. (eds.), *Methods in Paleomagnetism. Elsevier, Amsterdam*, 254-286.

896 Zubtsov, E.L., 1971. Late Precambrian Ulutau – Tien-Shan tillite complex. Moscow State
897 University, Moscow, 150 p. (in Russian).

898

899

900

901

902

Accepted Manuscript

903 Figure captions

- 904 Fig. 1. (a) Location of the Central Asian orogenic belt within Eurasia. (b) Generalized tectonic
 905 scheme of the CAO (the Altaids) and major surrounding units (simplified after
 906 Mossakovsky et al., 1993). Microcontinents (cross-hatched in Kazakhstan and black in South
 907 Siberia and Mongolia): AM, Aktau-Mointy; BA, Baydaric (or Dzabkhan); CM, Central
 908 Mongolian, CN, Chatkal-Naryn; CT, Central Tien Shan; DA, Derbi-Arzubey; GK, Great
 909 Karatau; JU, Junggar; KO, Kokchetav; LK, Lesser Karatau; M, Muya; NT, North Tien Shan;
 910 TB, Tarbagatay; TM, Tuva-Mongol; UL, Ulutau. Also labeled are the Lake tectonic zone (L)
 911 in west Mongolia and the Tuva area in South Siberia. The rectangle outlines the location of
 912 Fig. 2. Square denotes the study area on the Baydaric microcontinent (Levashova et al.,
 913 2010).
- 914 Fig. 2. Schematic geological map of the Lesser Karatau Range. The sampling localities are
 915 shown as solid circles and labeled as in the text.
- 916 Fig. 3. Schematic stratigraphic column for rocks in the Lesser Karatau microcontinent
 917 (thicknesses are arbitrary).
- 918 Fig. 4. (a) Concordia diagram for the lowermost tuff yielding an age of 831 ± 15 Ma (2σ). (b)
 919 Concordia diagram for the uppermost tuff yielding an age of 766.4 ± 7.2 Ma (2σ).
- 920 Fig. 5. Representative thermal demagnetization plots for the Kurgan rocks in stratigraphic
 921 coordinates. Full (open) circles represent vector endpoints projected onto the horizontal
 922 (vertical) plane. Temperature steps are in degrees Celsius. Magnetization intensities are in
 923 mA/m. Dashed lines denote isolated components labeled as in the text. NRM values are
 924 omitted from some plots for clarity.
- 925 Fig. 6. a-b, Stereoplots of ITC site-mean directions (circles) in situ (a) and after tilt correction
 926 (b); for clarity, confidence circles are not shown. Star is the ITC overall mean with
 927 confidence circle (thick line). Crosses are the reference directions for Baltica with confidence
 928 circles. Diamond is the Late Ordovician inclination for this area with confidence interval
 929 (shaded). c-d, Elongated distributions of unit ITC directions (small circles) in situ. Solid
 930 (open) symbols and solid (dashed) lines are projected onto lower (upper) hemisphere.
- 931 Fig. 7. a-b, Stereoplots of HTC site-mean directions (circles) with confidence circles (thin lines)
 932 in situ (a) and after tilt correction (b). Star is the HTC overall mean with confidence circle
 933 (thick line). Shaded triangles are three discarded sites, where adequate component separation
 934 is not achieved (see text for discussion). Inverted triangle in b is the overall ITC mean. c, Plot
 935 of concentration parameter for HTC site-means versus percent of unfolding. d-e, Stereoplots
 936 of the HTC mean directions with confidence circles for sections A (circle) and B (square) in
 937 situ (d) and after tilt correction (e). Other notation is as in Figure 6.

938 Fig. 8. Paleolatitude versus age plots for major cratons and the observed values for Kurgan tuffs
939 of the Lesser Karatau microcontinent (asterisk) and the Dzabkhan volcanics (large encircled
940 star with error bars) from Levashova et al. (2010). For major cratons, the symbols correspond
941 to the paleolatitudes of their centers, while the corresponding bands denote the paleolatitude
942 range covered by this craton (without error limits). If more than two points are available from
943 a craton, the symbols are connected by thick dashed lines for better visibility. The data are
944 numbered as in Table 4.

945 Fig. 9. Paleogeographic reconstruction for Tommotian time (simplified from Figure 7 in Meert
946 and Lieberman, 2008) showing provisional location of CAOB microcontinents with thick
947 carbonate covers and surrounding island arcs.

Accepted Manuscript

Table 1. Geochronologic Results from Rhyolitic Tuffs

Grain Name	$^{207}\text{Pb}/^{235}\text{U}^*$	2 σ % error*	$^{206}\text{Pb}/^{238}\text{U}$	2 σ % error	RHO (error corr.)	$^{207}\text{Pb}/^{235}\text{U}$ Age	2 σ error	$^{206}\text{Pb}/^{238}\text{U}$ Age	2 σ error	% discordance
Paleoproterozoic-										
K2006-2-2	6.29492	5.4	0.36299	4.6	0.86	2018	46	1996	78	1
K2006-2-4	6.33664	5.6	0.36908	5.0	0.88	2024	48	2025	86	0
K2006-2-6	6.27429	5.6	0.36454	4.4	0.81	2015	48	2004	76	1
K2006-2-9	6.39292	5.2	0.37263	4.2	0.83	2031	44	2042	74	-1
K2006-2-11	6.36096	5.4	0.37116	4.4	0.80	2027	48	2035	76	0
K2006-2-13	6.44249	6.4	0.37188	4.6	0.73	2038	56	2038	82	0
K2006-2-15	6.49849	5.4	0.37878	4.4	0.82	2046	48	2071	80	-1
K2006-2-19	6.38395	5.2	0.36769	4.6	0.89	2030	46	2019	80	1
K2006-2-20	6.52137	8.2	0.37549	6.4	0.80	2049	70	2055	114	0
K2006-2-26	6.39120	5.4	0.37164	4.6	0.85	2031	48	2037	80	0
Neoproterozoic										
K2006-2-1	1.26609	9.8	0.13543	5.4	0.54	831	56	819	40	1
K2006-2-5	1.18311	7.6	0.13010	5.6	0.75	793	42	788	42	1
K2006-2-3	1.27482	9.8	0.13794	5.2	0.52	835	56	833	40	0
K2006-2-17	1.37103	13.8	0.13628	6.6	0.48	877	80	824	52	6
K2006-2-18	1.31342	9.0	0.14071	4.8	0.52	852	52	849	38	0
K2006-2-23	1.33228	15.6	0.14013	4.8	0.32	860	88	845	38	2
K2006-2-25	1.31256	10.8	0.13981	5.0	0.46	851	62	844	40	1
Neoproterozoic										
K2006-4-1	1.14019	7.4	0.12630	3.4	0.45	773	40	767	24	1
K2006-4-2	1.11935	11.6	0.12317	2.4	0.20	763	62	749	16	2
K2006-4-3a	1.20440	10.4	0.13151	2.6	0.24	803	56	796	18	1
K2006-4-3b	1.17129	8.8	0.12829	3.4	0.39	787	48	778	26	1
K2006-4-4	1.09265	13.0	0.12126	4.0	0.31	750	68	738	28	2
K2006-4-5	1.12785	14.0	0.12429	3.2	0.23	767	74	755	24	1
K2006-4-6	1.12456	8.0	0.12482	2.6	0.31	765	44	758	18	1
K2006-4-8	1.17685	10.2	0.12777	3.8	0.37	790	56	775	28	2
K2006-4-9	1.18537	11.0	0.12826	3.0	0.26	794	60	778	22	2
Other Zircons										
K2006-2-8	14.60683	6.6	0.52902	5.8	0.88	2790	62	2737	130	2
K2006-2-10	11.68545	5.2	0.48177	4.6	0.88	2580	48	2535	98	2
K2006-2-12	7.67272	6.0	0.39741	4.2	0.71	2193	54	2157	78	2
K2006-2-22	12.20832	7.8	0.48906	5.6	0.71	2621	74	2567	118	2
K2006-2-24	8.65399	9.0	0.37200	6.6	0.74	2302	84	2039	120	11

Explanation: $^{207}\text{Pb}/^{235}\text{U}^*$ ratios and errors are calculated from measured $^{207}\text{Pb}/^{206}\text{Pb}$ and $^{206}\text{Pb}/^{238}\text{U}$, and known $^{238}\text{U}/^{235}\text{U}$ (1/137.88). All radiogenic ratios and ages are corrected for instrumental drift. $^{207}\text{Pb}/^{235}\text{U}$ and $^{206}\text{Pb}/^{238}\text{U}$ ratios and ages are corrected for U/Pb isotopic fractionation using the intercept method and common lead using the "207" method.

Table 2. Intermediate-temperature component data in the Kurgan rocks

Sites [#]	B°	N	In situ				Tilt-corrected			
			D°	I°	k	a ₉₅ °	D°	I°	k	a ₉₅ °
M1005	48/48	7/7	209.3	-48.2	43	9.4	215.1	-3.1	31	11.2
M1012	50/48	6/6	204.3	-24.8	92	7.0	205.4	19.3	48	9.8
M1018	49/49	7/6	210.9	-15.6	124	6.0	208.4	30.9	67	8.3
M1025	46/45	7/6	213.1	-11.4	20	15.2	211.0	32.9	26	13.4
M1032*	43/32	7/2	215.9	-28.9	-	-	216.7	2.9	-	-
M1039	20/31	7/5	199.1	-54.2	114	7.2	198.7	-22.9	176	5.8
M1048	22/33	8/7	206.3	-6.6	21	13.5	206.8	26.4	21	13.5
M1056	23/26	8/7	200.0	-23.9	72	7.2	200.2	3.9	73	7.1
M1064	11/27	7/7	197.6	-45.6	43	9.3	196.0	-19.0	54	8.3
M1071	36/37	7/7	214.9	-19.6	24	12.5	214.9	17.1	22	13.1
N4305-1	32/41	8/8	224.1	-56.5	38	9.1	218.8	-15.6	36	9.3
N4305-2	28/40	8/4	210.7	-0.5	106	9.0	211.4	39.9	93	9.6
N4313	36/38	8/4	205.7	5.1	190	9.1	201.8	42.4	190	9.1
N4321	46/34	9/6	215.6	-31.8	22	14.6	217.1	1.7	22	14.6
N4330*	39/31	8/2	216.3	-38.2	-	-	216.8	-7.2	-	-
N4338	41/31	9/6	214.1	-36.6	24	13.9	215.3	-5.7	24	13.9
N4347	17/35	5/4	199.4	-4.4	31	16.8	199.8	30.8	38	15.1
N4363-1	16/35	8/7	197.3	-55.8	88	6.5	196.7	-20.8	88	6.5
N4363-2	16/35	8/6	191.4	-24.6	42	10.5	191.7	10.3	42	10.5
N4371	22/42	8/8	202.1	-12.3	422	2.7	202.2	29.5	189	4.0
N4379	22/44	9/8	204.2	-14.9	122	5.0	204.4	29.1	138	4.7
N4387	22/44	8/8	205.5	-23.6	92	5.8	205.6	21.0	108	5.3
N4395	30/35	8/7	214.1	-58.1	11	18.7	212.2	-23.2	11	18.7
N4403	36/32	8/8	205.8	-29.8	59	7.3	207.1	1.7	76	6.4
N		(25/20)	207.0	-28.5	16	8.3	207.0	9.0	13	9.4
M1078	158/26	7/7	200.8	-34.2	107	6.0	219.5	-50.1	129	5.5
M1085	159/16	8/5	212.0	-58.2	119	7.1	239.5	-64.7	143	6.4
M1093	146/15	6/5	244.4	-64.7	60	10.2	270.7	-58.9	60	10.2
M1099*	144/18	7/6	211.5	14.0	10	21.7	209.1	4.2	11	21.1
M1106*	167/19	7/7	203.9	-21.9	6	25.8	212.3	-34.8	6	25.8
N4418	134/16	9/9	214.8	-34.4	91	5.5	226.1	-35.3	91	5.5

N4427	147/14	8/7	213.1	5.9	66	7.5	212.4	0.0	66	7.5
N4435	155/17	8/5	200.3	-56.3	219	5.2	226.8	-65.4	219	5.2
N4443	182/20	8/8	205.8	-9.1	60	7.2	208.7	-27.2	68	6.8
W		(10/7)	211.0	-36.8	8	21.9	224.7	-45.0	9	21.4
Mean		(35/27)	207.9	-30.6	14	7.8	210.4	-4.0	6	12.4
			$F_{(2, 50)} = 3.18$				$f = 0.74$			$f = 20.5$
Cobbles	26/90	13/11	220.8	-49.1	14	12.5	218.5	39.2	14	12.5

- not shown are the sites where no ITC is isolated or ITC directions are very scattered;

* - excluded from computation of the overall mean because of small statistics or low precision;

Comments: N and W are the sections with the dips to the northeast and southeast, respectively (Fig. 2); the entries N4305-2 and N4363-2 were not used in computation of the overall mean and are not shown in Figure 5a-b. B is the site's azimuth of dip/dip angle; N is the number of samples (sites) studied/accepted; D, declination; I, inclination; k, concentration parameter; α_{95} , radius of 95% confidence circle (Fisher, 1953).

Table 3. High-temperature component data in the Kurgan rocks

Sites [#]	B	N	In situ				Tilt corrected			
			D°	I°	k	a ₉₅ °	D°	I°	k	a ₉₅ °
M1005	48/48	7/7	202.8	20.9	16	15.8	176.0	59.9	23	13.1
M1012	50/48	6/6	203.8	12.4	94	7.0	184.2	52.9	113	6.3
M1018	49/49	7/6	16.0	-24.5	11	21.1	344.2	-58.2	14	19.2
M1025	46/45	7/5	211.5	24.3	31	15.9	191.9	66.3	46	13.0
M1032	43/32	7/5	197.9	30.6	78	9.4	180.1	57.7	78	9.4
M1039*	20/31	7/3	190.8	-78.6	59	19.0	196.9	-47.7	49	23.2
M1048	19/33	8/5	202.1	17.2	58	10.8	203.5	50.5	51	11.6
M1056	23/26	8/4	341.9	-24.8	69	11.1	328.5	-43.0	56	12.4
M1064	11/27	7/4	178.3	30.6	35	21.4	171.3	56.2	50	17.8
N4305	34/42	8/8	194.8	13.6	59	7.3	183.0	51.9	76	6.5
N4313	36/38	8/4	205.7	5.1	190	9.1	201.8	42.4	190	9.1
N4330	39/31	8/4	200.3	31.3	82	10.8	186.4	59.6	82	10.8
N4371	22/41	8/8	188.9	13.9	234	3.8	180.4	53.7	503	2.6
N4379	21/44	9/8	190.1	2.6	113	5.2	185.3	45.6	124	5.0
N4387	22/44	8/8	187.9	5.3	118	5.2	180.9	48.0	118	5.2
N		(25/14)	194.6	18.7	28	7.6	181.3	54.1	53	5.5
M1078	156/26	7/7	346.5	-64.1	110	6.2	342.0	-38.7	63	8.2
M1085-N	145/15	3/3	221.8	66.4	44	18.7	195.1	59.6	44	17.3
M1085-R	160/16	5/5	311.1	-71.9	59	10.4	324.0	-56.7	61	10.1
M1099	149/18	7/6	213.5	55.5	340	3.8	195.2	45.0	270	4.3
M1106 [§]	167/19	7/5	208.1	49.2	136	7.1	197.9	33.7	108	7.9
N4427 [§]	146/15	8/7	214.6	38.8	73	7.1	205.0	32.3	77	6.9
N4443 [§]	185/22	8/8	217.5	49.0	84	6.5	208.9	29.3	83	6.5
W		(10/7)	203.9	59.1	19	14.3	189.6	44.2	16	15.8
W1		(10/4)	189.8	68.4	22	20.2	174.0	52.0	20	21.2
Mean		(35/21)	196.3	31.8	11	9.9	184.1	50.9	28	5.9
Mean1		(35/18)	194.2	29.2	10	11.5	179.6	53.7	41	5.4
			$F_{(2,32)} = 3.29$		$f = 28.4$			$f = 0.44$		
Reverse		(4)	351.2	-48.3	8	36.1	334.8	-49.4	49	13.2
Normal		(14)	198.6	23.5	16	10.4	187.2	53.9	83	4.4

- not shown are the sites where no HTC is isolated or HTC directions are very scattered;

* - anomalous direction is excluded from computation of the overall mean.

W and Mean are calculated for all data; W1 and Mean1 are computed without three site-means marked with § (see text for discussion). Polarity assignments are arbitrary. Other notation is as in Table 2.

Accepted Manuscript

Table 4. Selected paleomagnetic poles

No	Rock unit	Age (Ma)	Pole		A ₉₅ ^o	Lat ^o	Reference
			Φ ^o	Λ ^o			
	India/Seychelles						
2	Malani rhyolites (IND)	761 ± 10	75	71	10	39N – 23N	Torsvik et al., 2001a
3	Mahe granites (SEY) ^e	755 ± 1	77	23	2	32N – 15N	Torsvik et al., 2001b
4	Mahe dykes (SEY) ^e	750 ± 3	80	79	16	34N – 18N	Torsvik et al., 2001b; Hargraves and Duncan, 1990
	Australia						
5	Hussar Formation	800 -760	62	86	10	3N – 19S	Pisarevsky et al., 2007
6	Mundine dykes	755 ± 3	45	135	4	31N – 8N	Wingate and Giddings, 2000
7	Walsh Tillite	750 -770	22	102	14	44N – 19N	Li, 2000
	Yaltipena Formation ^c	620 - 630	44	173	8	27N – 5N	Sohl et al., 1999
	Elatina Formation ^c	600 - 620	39	186	9	26N – 1N	Sohl et al., 1999
	Brachina Formation ^c	~580	33	148	16	44N – 20N	McWilliams and McElhinny, 1980
	Lower Arumbera/ Pertataka Formation ^c	~570	44	162	10	30N – 7N	Kirschvink, 1978
	Upper Arumbera SS ^c	~550	46	157	4	30N – 6N	Kirschvink, 1978
	Todd River	~530	43	160	7	32N – 9N	Kirschvink, 1978
	South China						
8	Xiaofeng dykes	807 ± 10	14	91	11	~69N	Li et al., 2004
9	Liantuo Formation	748 ± 12	4	161	13	~37N	Evans et al., 2004
10	Nantuo Formation ^d	~740	0	151	5	~43N	Rui and Piper, 1997
	Meishucun Formation ^d	~525	9	31	10	~14N	Lin et al., 1985
	Tianheban Formation ^d	~511	-7	10	23	~12S	Lin et al., 1985
	Hetang Formation ^d	~511	-38	16	17	~18S	Lin et al., 1985
	North China						
11	Nanfen Formation	800 - 780	-16	121	11	~39N	From Zhang et al., 2006
	Mean pole	~700	-43	107	6	~11N	From Zhang et al., 2006
	Donjia Formation, Lushan	~650	-61	97	7	~8S	From Zhang et al., 2006
	Tarim						
12	Aksu Dykes	807 ± 12	19	128	6	~43N	Chen et al., 2005
13	Baiyixi Formation	~740	17	194	4	6S	Huang et al., 2005
	Laurentia						
14	Galeros Formation	780 - 820	-2	163	6	21N – 25S	Weil et al., 2004
15	Wyoming dykes	782 ± 8; 785 ± 8	13	131	4	23N – 36S	Harlan et al., 1997
16	Tsezotene sills and dykes	779 ± 2	2	138	5	16N – 34S	Park et al., 1989
17	Kwagunt Formation	742 ± 6	18	166	7	41N – 6S	Weil et al., 2004
18	Natkusiak Formation	723 ± +4/-2	6	159	6	27N – 20S	Palmer et al., 1983; Heaman et al., 1992
19	Franklin dykes	723 ± +4/-2	5	163	5	27N – 19S	Heaman et al., 1992; Park, 1994

	Long Range Dykes ^a	620 - 610	19	355	18	34N – 6S	Murthy et al., 1992; Kamo and Gower, 1994
	Callander complex	575 ± 5	-46	121	6	34S – 81S	Symons and Chiasson, 1991
	Catochin Basalts-A	564 ± 9	-42	117	9	32S – 77S	Meert et al., 1994 a,b
	Sept-Iles complex B ^b	564 ± 4	-44	135	5	27S – 74S	Tanszyk et al., 1987
	Siberia						
20	Karagas Series	850(?) -740	-12	97	10	22N – 8N	Metelkin et al., 2005
21	Nersinsky complex	~740	-37	122	11	2N – 19S	Metelkin et al., 2005
	Mean pole for V _{2edc}	~560	-35	77	6	3S – 16S	Shatsillo et al., 2006
	Redkolesnaya Fm.	~550	-61	68	5	30S – 42S	Shatsillo et al., 2006
	Mean pole for the Nemakit-Daldynian stage	~540	-60	115	7	25S – 41S	Shatsillo et al., 2006
	Mean pole for Cam ₁	~525	-48	151	8	19S – 36S	Shatsillo et al., 2006
	Baltica						
22	Hunedalen dykes	~848	-41	222	10	59S – 87S	Walderhaug et al., 1999
	Egersund dykes	~608	-31	224	15	50S – 81S	Walderhaug et al., 2007
	Mean pole	~555	-30	298	10	4S – 31S	Popov et al., 2002; Iglesia-Llanos et al., 2004; Popov et al., 2005
	Tornetrask Formation	~535	-56	296	12	24S – 52S	Torsvik and Rehnstrom, 2001

Comments: No, numbers of the results that are used in Figure 8. Pole, coordinates of the north paleomagnetic pole: Φ , latitude (positive for northern hemisphere); Λ , longitude (east). A_{95} , radius of confidence circle around paleomagnetic pole. Lat, the range of paleolatitudes, which were occupied by a craton.

^a Recalculated by Hodych et al., (2004)

^b The Sept-Iles complex “B” direction (after correction for minor tilt – see Symons and Chiasson, 1991) matches other ~570 Ma poles from Laurentia, while “A” direction falls close to the Cambro-Ordovician segment of the North American APWP (see Meert et al., 1994)

^c Estimated age based on stratigraphic information given in Pisarevsky et al., (2001) and stable isotope calibration given in Walter et al., (2000)

^d Estimated age based on known isotopic and/or stratigraphic position

^e Rotated to India according to Torsvik et al. (2001b)

Abbreviations: IND, India; SEY, Seychelles

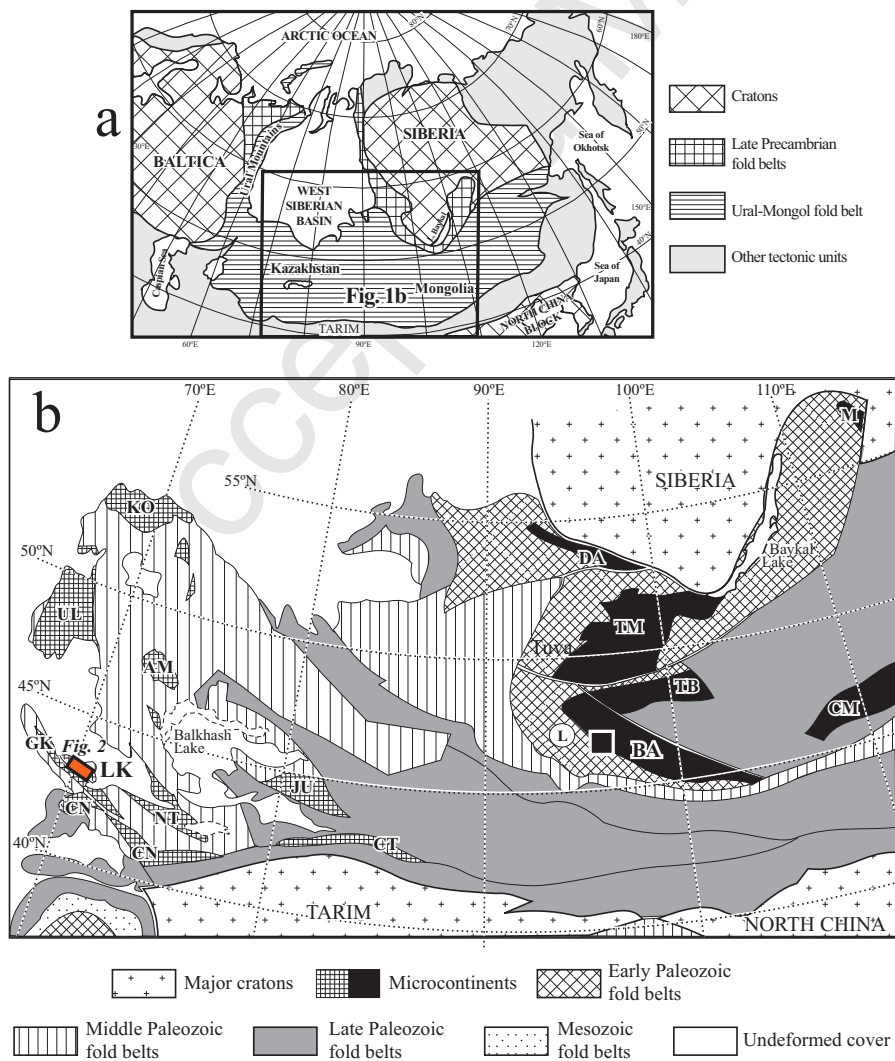
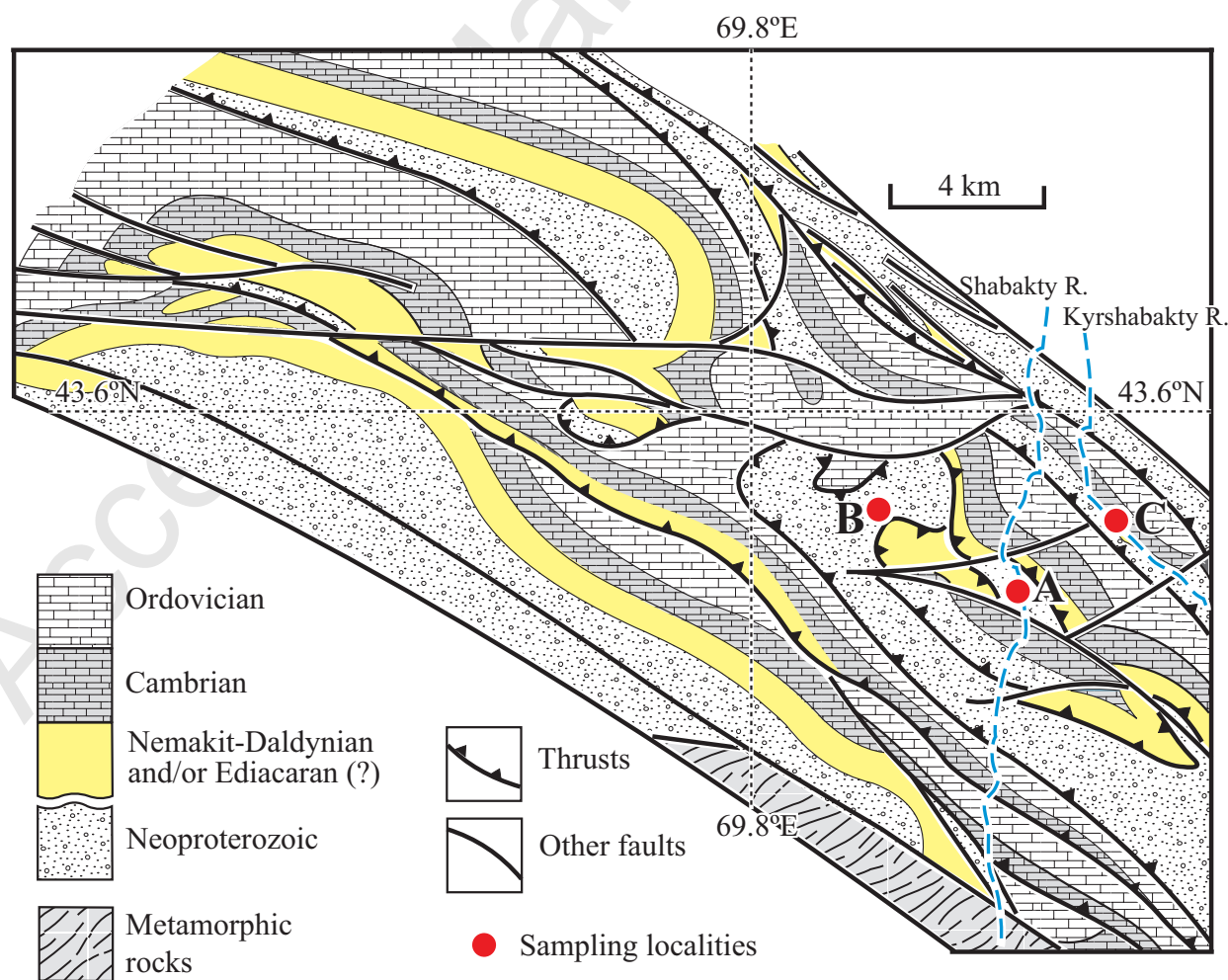
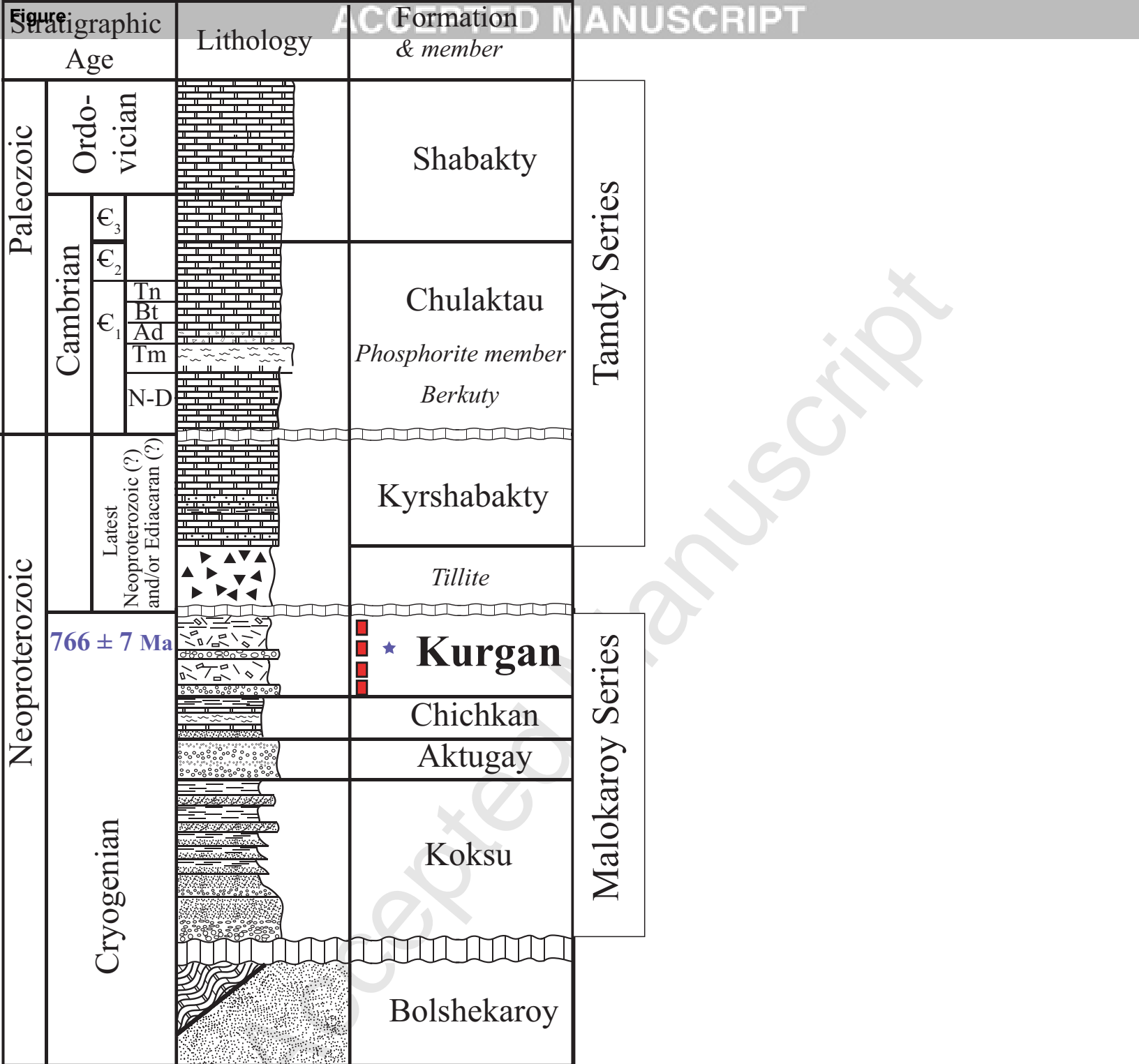


Fig. 1, Levashova et al.





■ Paleomagnetic Sites

★ Geochronology Site

Fig. 3 Levashova et al.

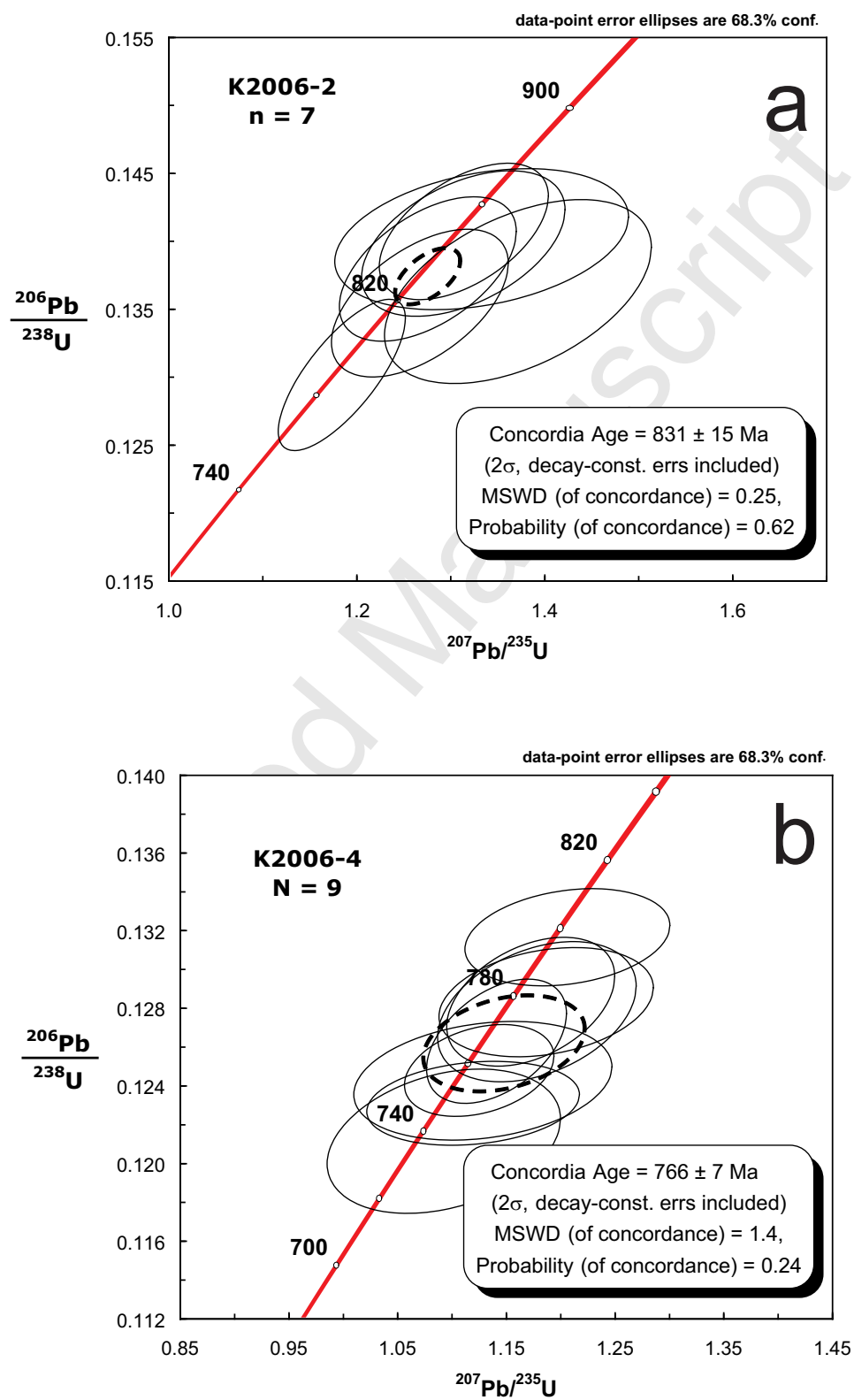


Fig. 4 Levashova et al.

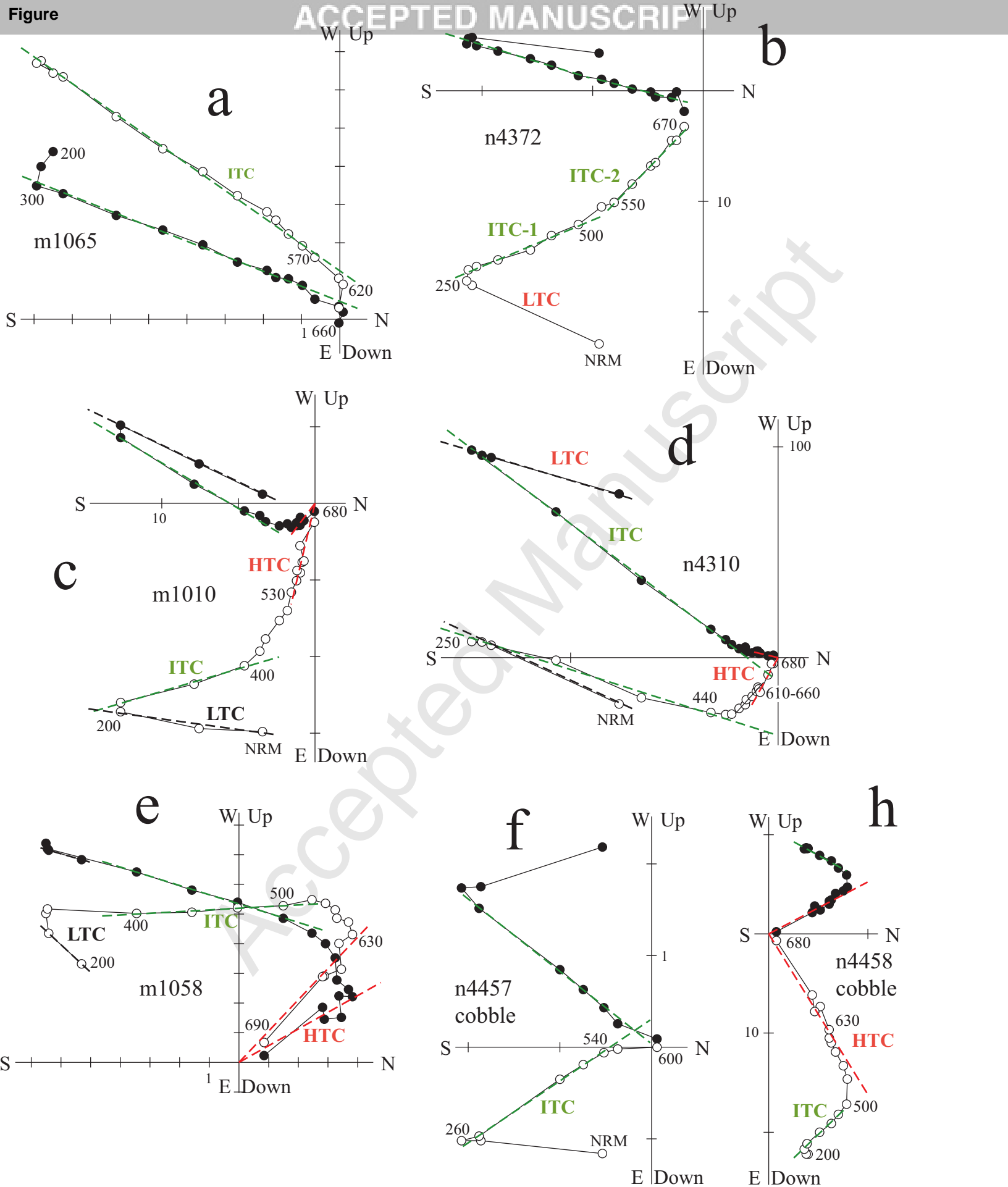
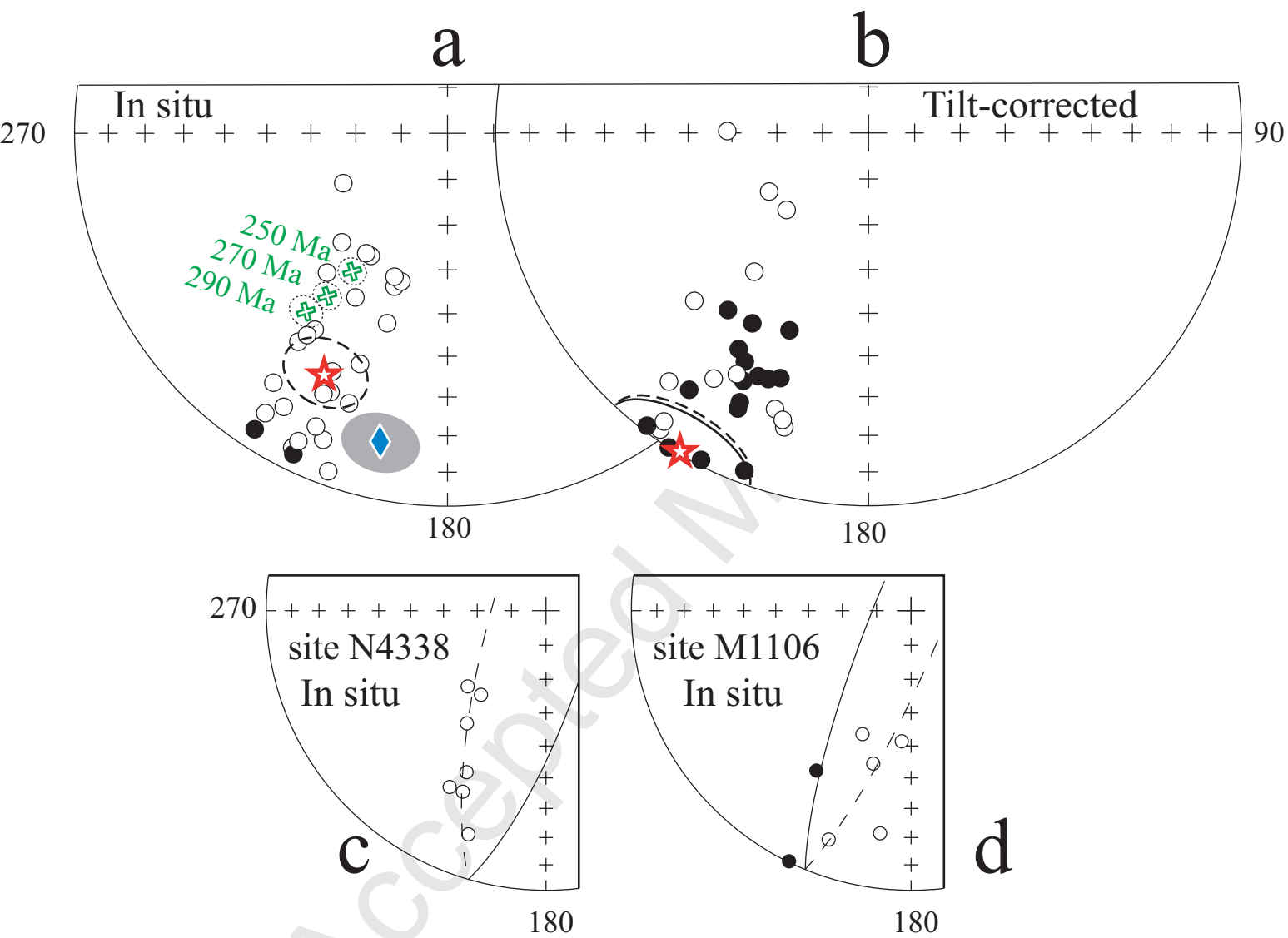
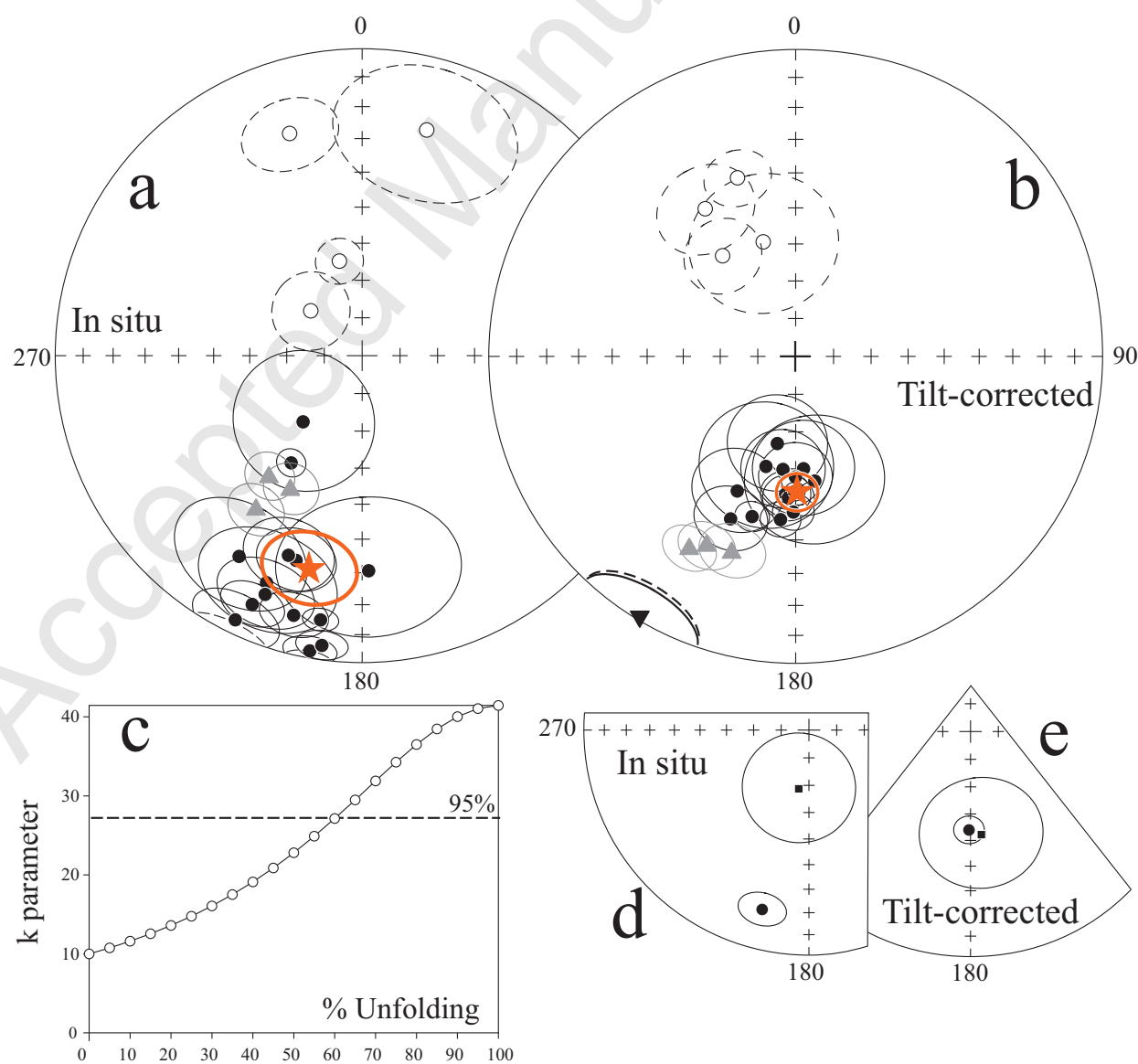


Fig. 5, Levashova et al.





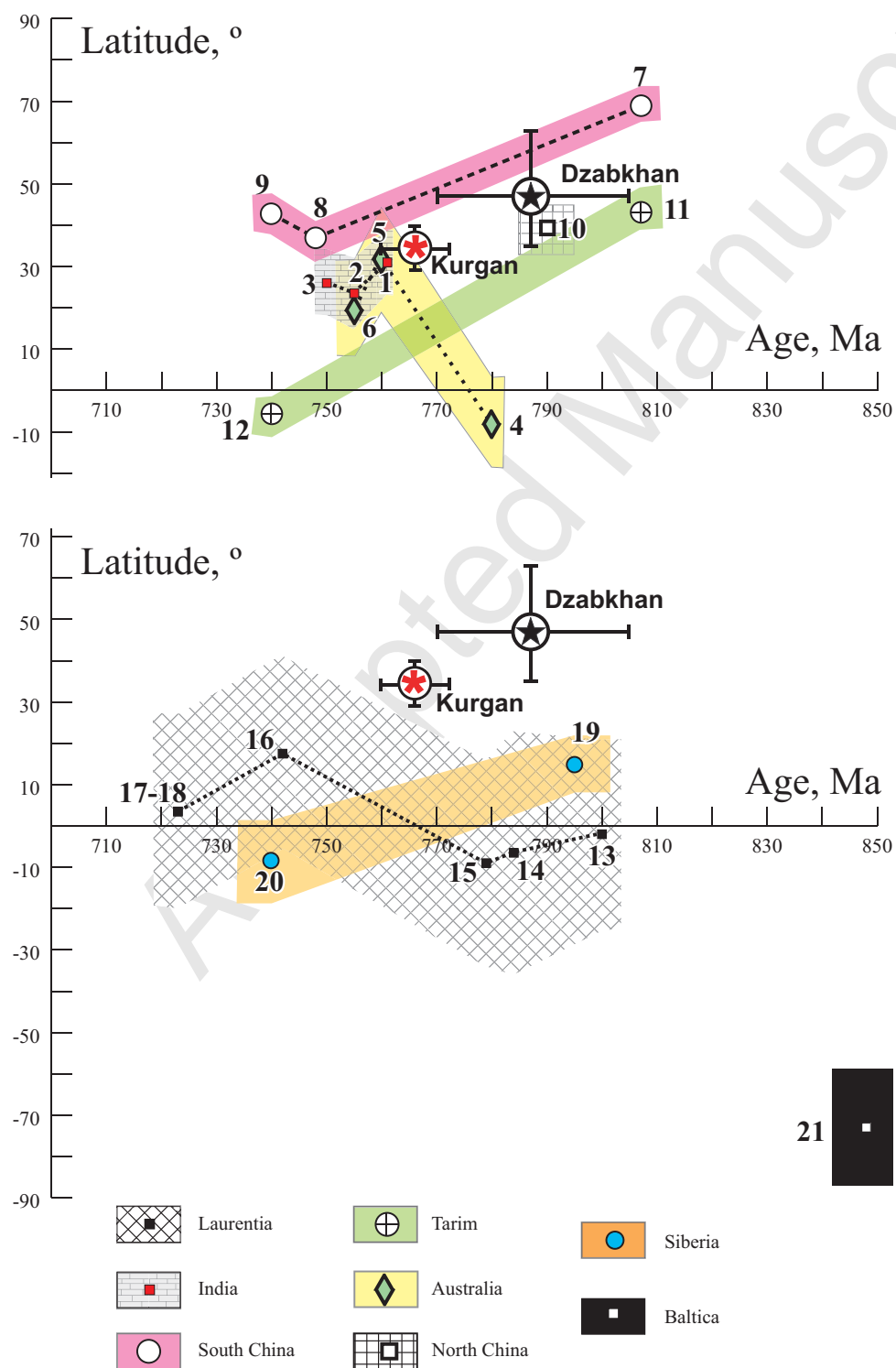


Fig. 8 Levashova et al.

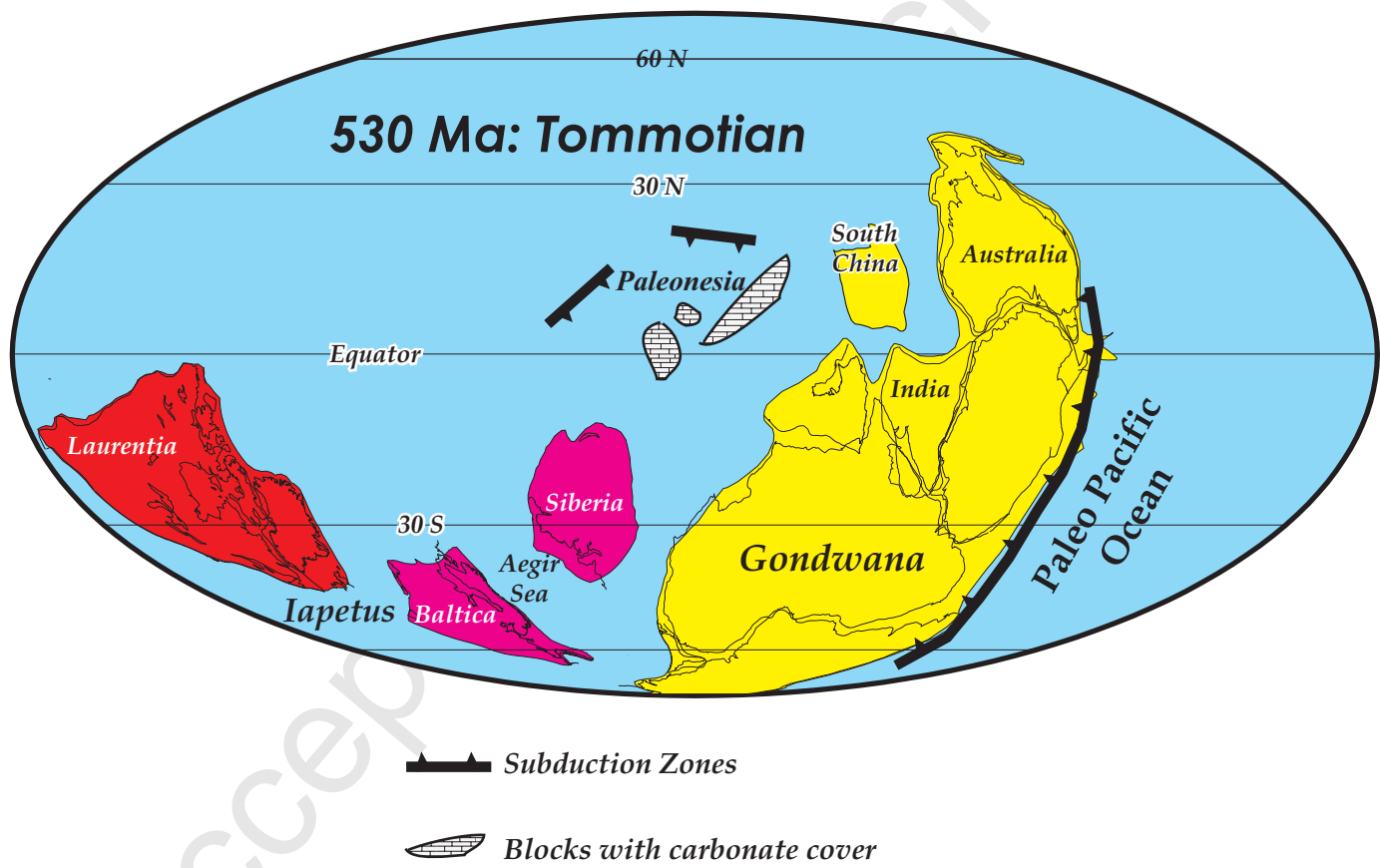


Fig. 9 Levashova et al.